Synaptic noise induces intermittent oscillatory-quiescent state transitions in a spiking network model

Rodrigo F. O. Pena[1*], Michael A. Zaks[2☯], Antonio C. Roque[1☯]

1 Dept of Physics, Faculty of Philosophy, Sciences and Letters of Ribeirão Preto, University of São Paulo, Ribeirão Preto, SP, Brazil
2 Dept of Physics, Faculty of Mathematics and Natural Sciences, Humboldt University of Berlin, Berlin, Germany

☯These authors contributed equally to this work.
* rfdop@uol.com.br

Abstract

Spontaneous cortical population activity is often described as synchronous during slow-wave sleep and under certain anesthetics, and asynchronous during quiet wakefulness. The underlying mechanisms that control transitions between these cortical states are not completely known. To study the effect of synaptic noise on these transitions, we use a cortical network model with mixed neuronal types, governed by deterministic equations, and introduce noise into the dynamics of synaptic variables. In absence of noise, the network is known to display spontaneous collective oscillations which resemble alternating up and down states observed in synchronous cortical states. Records of noise-affected activity in the network feature alternation of collective oscillations and quiescent states, with irregular transitions between them. Systematic analysis of firing rates, power spectra and voltage series shows that characteristics of these two states are similar to those of synchronous and asynchronous cortical states: in the synchronous-like state neurons display collective oscillatory activity and their membrane voltages fluctuate between hyperpolarized (down) and depolarized (up) states; in the asynchronous-like state neurons are weakly correlated and display very low spiking activity with no collective dynamics. By varying noise intensity and using mean duration at each state as a prevalence criterion, we observe that noise facilitates transitions from the asynchronous to the synchronous-like state and hinders the reverse transitions. Our results suggest that synaptic noise may be an important mechanism underlying transitions between asynchronous and rhythmic states in cortical networks.

Author summary

Recordings of brain activity show that the same neuronal population may generate diverse firing patterns ranging from collective bursting oscillations to irregular and uncoordinated spiking. These neuronal patterns correlate to global brain states like sleep and wakefulness, hinting that they may have some kind of functional significance. We show here that a network of spiking neuron models with parameters tuned to reproduce intrinsic firing patterns of cortical neurons is able to display oscillatory and non-oscillatory firing patterns, which bear resemblance to observed cortical activity states. Moreover, we show that synaptic noise causes spontaneous intermittent transitions between oscillatory and quiescent non-oscillatory regimes. The time duration

of each regime depends on the synaptic noise intensity and the intrinsic firing characteristics of the neurons in the network. Our results point to a bridge from events at the molecular scale of synapses to the cellular scale of individual neurons to the collective scale of neuronal populations.

1 Introduction

Studies in which large neuronal populations are simultaneously recorded disclose complex spatio-temporal firing patterns characterized by rhythmic oscillations with variable degrees of synchrony [1–4]. Recent evidence suggests that in the cortex these patterns form a continuum of states ranging from a "synchronized" state, characterized by low-frequency oscillation in the population firing rate and up/down switching in the single-neuron membrane potential, to a "desynchronized" state, marked by a roughly constant population firing rate and irregular single-neuron firing [5–9]. Synchronous states are more prominent during slow-wave sleep and anesthesia whereas asynchronous firing activity is prevalent in the state of wakefulness and in REM sleep [10–13]. Notably, the degree of synchrony in cortical and subcortical regions varies with time, often with intermittent switches between synchronous and asynchronous states [14–16].

There is a widespread assumption that prevalence of synchrony or asynchrony in the network activity depends on the relative strength of excitatory and inhibitory synaptic inputs [17–20]. In the context of networks of leaky integrate-and-fire (LIF) neurons, the balance between average excitatory and inhibitory synaptic inputs is known to result in quantitative characteristics of network activity that resemble those of asynchronous cortical states [21–28]. In the absence of such balance, the network displays behaviors akin to synchronous cortical states [29].

Networks in which the nodes feature more complicated dynamics than LIF neurons and are able to reproduce intrinsic firing patterns of contrasting cortical neurons, e.g. based on the Izhikevich [30, 31] or the AdEx [32, 33] models, demonstrate higher diversity of temporal patterns. In the region of parameter space where inhibition exceeds excitation, mixtures of neurons with different individual firing characteristics perform collective spontaneous oscillations that resemble the alternation of up and down states observed in the synchronized cortical state [34, 35]. This suggests that not only excitation/inhibition balance but also heterogeneities in the neuronal composition of the network may have an impact on the dynamic pattern of the network.

Yet another factor, capable of influencing the interplay between oscillatory and non-oscillatory states, is the intrinsic randomness of synaptic channels. Spontaneous firing of cortical neurons is irregular, and its stochasticity is known to play an important role in cortical dynamics [36–41]. In particular, synaptic noise, which has been identified as a major noise source for cortical neurons [42], may trigger excursions of network dynamics across different states. In fact, sensory inputs can provoke transitions between up and down states [43, 44] and the intrinsic mechanisms of these transitions can be related to processes at the synaptic level [45–47]. Consequently, it has been claimed that noise plays an important role in transitions between up and down states [48, 49]. More specifically, synaptic noise in the form of unreliable neurotransmitter release or as miniature excitatory postsynaptic currents (mEPSCs) has been demonstrated to have characteristics like frequency and amplitude that depend on the sleep/wake state [50].

In this study we show that a network of Izhikevich neurons with stochastic synaptic inputs displays spontaneous transitions between active states, characterized by rhythmic alternations of tonic firing and silence, and quiescent states with low-rate, irregular network firing. Moreover, in the active states the average neuronal membrane voltage oscillates between depolarized and hyperpolarized states in a manner that resembles cortical up/down oscillations whereas during the quiescent states the average membrane

potential remains close to the resting value. The study highlights the importance of synaptic noise and confirms that networks of non-LIF stochastic neurons display rich intrinsic dynamics.

2 Materials and methods

2.1 Neuron and network model

Our work is based on a recent model used to describe self-sustained oscillations across up and down states [34,35]. This is the standard random network model where directed connections between every two nodes are created with a fixed probability p. To keep cortical sparseness we have chosen a small connection probability $p = 0.01$ and size $N = 2^{10}$. This renders the expected number of incoming connections per node (average in-degree) $p(N-1) \approx 10$. The network is mixed: it includes both excitatory and inhibitory nodes. The sizes of excitatory and inhibitory subpopulations are chosen to be in the proportion $4:1$ [21]. Each node of the network is a neuron modeled by the Izhikevich formalism [30] with parameters that ensure diverse dynamics on the individual level. Every neuron is described by two variables: voltage $v(t)$ and membrane recovery variable $u(t)$, which follow the coupled differential equations

$$\begin{cases} \dot{v} &= \alpha v^2 + \beta v + \gamma - u + I(t) \\ \dot{u} &= a(bv - u), \end{cases} \tag{1}$$

with a fire and reset rule. Every time when $v(t)$ assumes the threshold value $v(t) = v_{\text{peak}}$, both variables are instantaneously updated:

$$\begin{cases} v(t) &\to c, \\ u(t) &\to u(t) + d. \end{cases} \tag{2}$$

Our choice of the Izhikevich neuronal model is based on its ability to mimic, by means of setting the appropriate values of parameters a, b, c, d, the behavior of neurons from different electrophysiological classes [75,76]. Among those, we concentrate in this study on the excitatory regular spiking (RS) and chattering (CH) neurons, and on the inhibitory fast spiking (FS) and low-threshold spiking (LTS) neurons. Examples of individual dynamics for the different classes are shown in Fig 1: the neuronal types differ in frequency, adaptation, and in rheobase current. We consider network compositions where all inhibitory neurons belong to the same class: all of them are either of the LTS type or of the FS type. In the excitatory subpopulation we consider the case when all neurons belong to the RS type, and the case when there is a mixture of RS with CH neurons.

The dynamics of the individual neuron model can be understood through its phase plane description. A thorough discussion of different properties of the Izhikevich neuron model can be found in [31].

The last term in the first equation of (1) describes the synaptic current which, for a neuron j, reads:

$$I_{syn,j}(t) = G_j^{\text{ex}}(t)\,(E_{\text{ex}} - v_j) + G_j^{\text{in}}(t)\,(E_{\text{in}} - v_j)\,. \tag{3}$$

The current is controlled by conductances $G_j^{\text{ex/in}}$ and reversal potentials $E_{\text{ex/in}}$, responsible for excitatory/inhibitory effects. Whenever an excitatory (inhibitory) neuron spikes, an increment g_{ex} (g_{in}) is added to the conductances G^{ex} (G^{in}) of all its postsynaptic neurons; thereafter the conductances decay exponentially with time

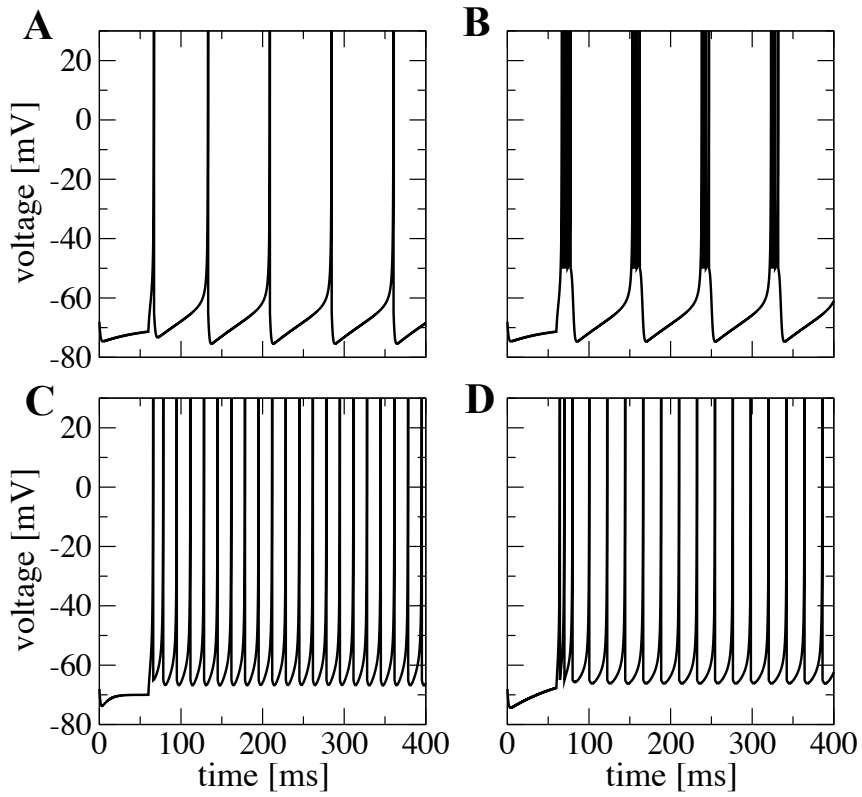

Fig 1. Electrophysiological cell classes modeled by the Izhikevich formulation. **A** excitatory neuron RS. **B** excitatory neuron CH. **C** inhibitory neuron FS. **D** inhibitory neuron LTS. Plots where produced with constant $I = 6$.

constant $\tau_{\mathrm{ex/in}}$. This is well known as a conductance based synaptic model, described by the differential equation

$$\frac{dG_j^{\mathrm{ex/in}}(t)}{dt} = -\frac{G_j^{\mathrm{ex/in}}(t)}{\tau_{\mathrm{ex/in}}} + g_{\mathrm{ex/in}} \sum_i \delta(t - t_i) + \sqrt{2Dn_j}\xi_j(t), \tag{4}$$

where summation is performed over all time instants t_i of preceding presynaptic spikes. We adopt the same parameters as in [35]: $E_{\mathrm{ex}} = 0$ mV, $E_{\mathrm{in}} = -80$ mV, $\tau_{\mathrm{ex}} = 5$ ms and $\tau_{\mathrm{in}} = 6$ ms; if not stated otherwise, the conductance increments are set to the values $g_{\mathrm{ex}} = 0.15$ and $g_{\mathrm{in}} = 1$.

The last term in Eq.(4) is the synaptic noise source. Since, for simplification, the noise sources are treated as being independent or weakly correlated, a superposition of a large number of such inputs is approximated by a simple Gaussian white noise process. We assume that ξ_j is Gaussian with $\langle \xi(t) \rangle = 0$ and $\langle \xi(t)\xi(s) \rangle = \delta(t - s)$. Since the sum of independent random normally distributed variables is normally distributed as well, the overall variance of the stochastic process for a neuron j is proportional to the total number of excitatory/inhibitory inputs n_j that this neuron receives. Thereby, for neurons with different numbers of presynaptic partners, the intensity of the noisy input is different. The conductances $G_j^{\mathrm{ex/in}}(t)$ of each neuron are modeled as stochastic Ornstein-Uhlenbeck processes [65]. This stochastic model, similar to the point-conductance model described in [63], has its power-spectral density and variance completely determined [64].

The complete set of parameter values used in the simulations of this study is summarized in Table 1.

Table 1. Parameters used in the simulations.

Common parameters in Eq.(1)	α	β	γ	v_{peak} [mV]
	0.04	5	140	30

Parameters of (1) for different firing patterns	**a**	**b**	**c [mV]**	**d**
Excitatory RS	0.02	0.2	-65	8
Excitatory CH	0.02	0.2	-50	2
Inhibitory FS	0.1	0.2	-65	2
Inhibitory LTS	0.02	0.25	-65	2

Synaptic parameters	$g_{\text{ex}}^{\max}$	$g_{\text{in}}^{\max}$	τ_{ex} [ms]	τ_{in} [ms]	E_{ex} [mV]	E_{in} [mV]
	0.15	1	5	6	0	-80

Network parameters	size N	ratio exc:inh	connectivity
	2^{10}	4:1	$p = 0.01$

2.2 Measures

In this subsection, we introduce neuron and network measures that will be used below for characterization of the results.

We start by defining the network time-dependent firing rate as

$$r(t;\Delta t) = \frac{1}{N\Delta t}\sum_{j=1}^{N}\int_{t}^{t+\Delta t} x_j(t')dt', \tag{5}$$

where the spike train x_j for each neuron j is viewed as a series of δ functions: $x_j(t) = \sum_{t_j^f}\delta(t-t_j^f)$, with $\{t_j^f\}$ being the set of times when neuron j fired. We fixed the time window $\Delta t = 1$ ms.

We will use two power spectra: the spike train power spectrum and the voltage time series power spectrum. The first one is defined for each neuron j as

$$S_{xx,j}(f) = \frac{\langle \tilde{x}_j \tilde{x}_j^* \rangle}{T}, \tag{6}$$

where $\tilde{x}_j(f)$ is the Fourier transform $\tilde{x}_j(f) = \int_0^T dt e^{2\pi i f t} x_j(t)$, $\tilde{x}_j^*$ is the complex conjugate and T is the length of the time interval. The power spectrum of the voltage time series is obtained in the same way, replacing in (6) the spike train $x_j(t)$ by the voltage time series $v_j(t)$. In the case of the spike train power spectrum the units are 1/s whereas the units of the voltage times series spectrum are mV^2/s.

To estimate the average power spectrum, we average the spectrum over a subset that includes K neurons:

$$\bar{S} = \frac{1}{K}\sum_{j\in K} S_{xx,j}(f), \tag{7}$$

To quantify the degree of oscillatory activity in the network, we use the spectral entropy H_s [67,68]. From the network time-dependent firing rate (Eq.(5)), the spectral entropy is computed as

$$H_s = \frac{-\sum_k S_k \log S_k}{\log N_b}, \tag{8}$$

where N_b is the number of frequency bins and S_k is the power spectrum of the network time-dependent firing rate at the kth bin. In our simulations we use N_b=1000 and normalize S_k so that $\sum_k S_k = 1$. In the case of broadband noise activity, the power spectrum of the network firing rate is flat and the spectral entropy is maximal $H_s = 1$. On the other hand, if all power is concentrated in one frequency, a case of single-frequency network oscillations, the spectral entropy vanishes: $H_s = 0$.

To quantify the degree of synchrony in the network, we use a measure based on the pairwise cross-correlation function $C_{ij}(\tau) = \langle x_i(t)x_j(t+\tau)\rangle - \langle x_i\rangle\langle x_j\rangle$, where $\langle . \rangle$ is used here to represent time average and $\langle x_i\rangle$ and $\langle x_j\rangle$ are, respectively, the mean values of the spike-trains of neurons i and j. Unless otherwise stated, the time average used to calculate C_{ij} is always taken over a simulation interval of $T = 2000$ ms. We define the synchrony index Σ as the integral of the cross-correlation function over a small window of length δ around zero [51] averaged over K neuron pairs

$$\Sigma = \frac{1}{K}\sum_{\{ij\}}^{K}\int_{-\delta}^{\delta} d\tau C_{ij}(\tau). \tag{9}$$

Synchronous network states are characterized by high values of the pairwise cross-correlation function whereas asynchronous states are characterized by low values of the pairwise cross-correlation function [52], so the average in Eq. (9) over a sufficiently large number K of neuron pairs results in high values for synchronous states and low values for asynchronous ones. In our simulations, we constructed parameter space plots of the synchrony index (like the ones shown in Results) for different values K of neuron pairs and observed a saturation in the plots for increasing values of K above 30. This indicates that the synchrony index value becomes independent of the number of neuron pairs for $K \geq 30$. To ensure this independence, in computations we used $K = 100$. The value of δ used in Eq.(9) was 1 ms. In our simulations, the value of the synchrony index ranged from near zero to above 3 (Σ is unbounded from above), and we chose $\Sigma = 0.1$ as the threshold to separate asynchronous from synchronous states with varying degrees of synchrony.

Numerical integration of the differential equations was performed by means of the Heun algorithm [66]. We used C++ to write the computational code, and Matlab and xmgrace to visualize and analyze the results.

3 Results

3.1 Preliminaries and the deterministic setup

To single out the effects caused by the introduction of synaptic noise, we first characterize the system in the non-perturbed state, i.e. in the absence of noise. Below, we refer to this case as the deterministic setup.

At the chosen parameter values the global state of rest is stable. Since in the deterministic setup no activity can be excited from that state without an initial disturbance, we start simulations by applying brief electric stimulation to arbitrarily selected neurons. Different stimuli are constructed by varying

- the amplitude of the input current from $I_{\rm stim} = 10$ to $I_{\rm stim} = 20$;
- the duration of the input current from $t_{\rm stim} = 50$ ms to $t_{\rm stim} = 300$ ms; and

- the proportion of stimulated neurons: 1, 1/2, 1/4, 1/8, 1/16.

The initial kick provided by brief stimulation has a sole role to put the system into a state other than rest. After the end of the stimulation, the network is left to evolve freely and its dynamics is recorded. Eventually all trials end up in the state of rest, but in most cases evolution is not a straightforward decay but a long dynamical transient; its duration strongly (by several orders of magnitude) varies, depending on the initial conditions. On discarding the cases where the free activity was shorter than 400 ms, we are left with a set of trials in which the network displayed long-living self-sustained activity.

We have studied different combinations of the conductance increments$(g_{\rm in}, g_{\rm ex})$ and observed rather distinct behavior as shown in Fig 2. The choice of $g_{\rm ex}$ and $g_{\rm in}$ directly affects the network balance and shapes thereby its dynamics [29].

Depending on the ratio g_{in}/g_{ex}, the self-sustained activity displayed by the network belongs to one of two categories as reported in [34]. The first one, shown in the left column of Fig 2, is a relatively constant network activity state where neurons spike in a synchronous but non-oscillatory fashion. This is confirmed by the high values of the spectral entropy ($H_s = 0.87$) and the synchrony index ($\Sigma = 0.50$) for the given example. The reason for the high synchrony of this state can be seen from the behavior of the voltage traces for two randomly selected neurons at the bottom of the left column of Fig 2: the neurons fire irregularly, but their firing rates are so high that the probability of finding spikes from both of them within a time window of 2 ms is high.

The second category, shown in the right column of Fig 2, is an oscillatory state ($H_s = 0.39$) characterized by regular periods of high mean firing rate intercalated with periods of very low firing. The average voltage indicates that the bulk of neurons is fluctuating between depolarization and hyperpolarization. The synchrony index for this state is not as high as for the constant activity state ($\Sigma = 0.19$), but neurons still fire in synchrony. To estimate the degree of synchrony of the high and low activity phases of the oscillations, we manipulated the raster plot to produce two new artificial raster plots: one containing only the high activity phases and the other containing only the low activity phases "glued" together. This gave $\Sigma = 0.18$ for the "high-activity" raster, and $\Sigma = 0.005$ for the "low-activity" raster. Hence, the network activity is synchronous during the high activity phases, and asynchronous during the low activity phases. Voltage traces for two randomly picked neurons (see bottom plot in the right column of Fig 2) show bursts of closely spaced spikes during high activity phases intercalated with periods of hyperpolarization below the reset value during low activity phases. This behavior was explained by us earlier [35] in terms of the dynamics of the recovery variable u in the single neuron phase plane of the Izhikevich neuron.

The example given in the middle column of Fig 2 illustrates the transition between the two above categories. This transition occurs when the level of inhibition overcomes the excitation as reported in [34]. The network activity in the transition region looks as a mixture of constant and oscillatory activity, with rather synchronous neuronal firing ($\Sigma = 0.48$) and strongly fluctuating mean firing rate ($H_s = 0.56$). Voltage traces for two randomly chosen neurons (bottom of middle column) show high firing rates, and thus high synchrony degree like in the first category (constant activity), but now there are short periods of activity break as in the second category (oscillatory activity).

Naively, $g_{in}/g_{ex} = 4$ may seem to be a balanced situation, as reported elsewhere [21]. Here, however, we are dealing with neurons from different electrophysiological classes, and their firing rates differ as well. The mean synaptic input for a given neuron j can be roughly estimated as

$$I_j(t) \approx g_{\rm ex} C_{\rm ex} \nu_{\rm ex} - g_{\rm in} C_{\rm in} \nu_{\rm in}, \tag{10}$$

where $C_{\rm ex/in}$ are the numbers of excitatory/inhibitory inputs to neuron j, and $\nu_{\rm ex/in}$ are the mean firing rates of the excitatory/inhibitory populations. Usually, when LIF

neurons are considered, equal mean firing rates of excitatory and inhibitory neurons are assumed, hence the balance requires that $g_{\rm in}/g_{\rm ex} = C_{\rm ex}/C_{\rm in}$, which, in the widely studied situation with the number of excitatory connections four times higher, results in $g_{\rm in}/g_{\rm ex} = 4$. In contrast, in a network like ours, with $\nu_{\rm in} > \nu_{\rm ex}$, there is no balance at $g_{\rm in}/g_{\rm ex} = 4$: inhibition is higher than excitation for this case.

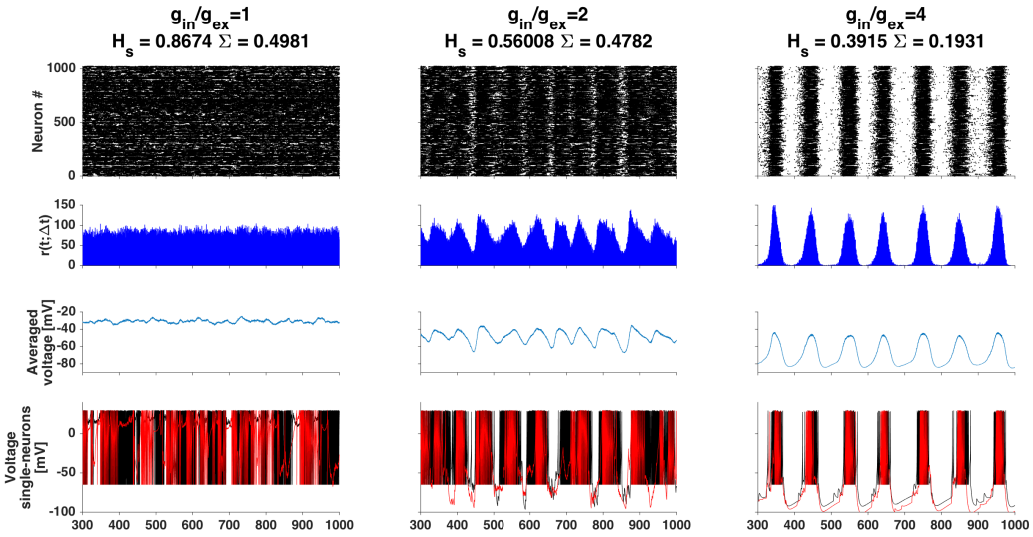

Fig 2. Self-sustained firing pattern changes under variation of $g_{\rm in}/g_{\rm ex}$ ratio in the deterministic setup. The network is composed of RS and LTS neurons. Each column represents a combination of $g_{\rm in}/g_{\rm ex}$ indicated atop together with the corresponding spectral entropy H_s and synchrony index Σ. From top to bottom: raster plot, network firing rate, average voltage and voltage traces of two arbitrarily selected neurons (in black and red respectively).

Altogether, these preliminary examples confirm that the deterministic setup, depending on the ratio $g_{\rm in}/g_{\rm ex}$, is able to generate oscillatory or constant activity. In the following, we concentrate on the oscillatory situation, when inhibition overcomes excitation.

In Fig 3 we present an exemplary simulation in the deterministic setup and extended statistics from the set of long-lived realizations with synaptic increments $g_{\rm ex} = 0.15$ and $g_{\rm in} = 1$ (this set contains 487 simulations, thus allowing good statistics). In this case the majority of neurons oscillates between a depolarized state and a hyperpolarized state, well visible in Fig 3 **B** and on the bimodal distribution in Fig 3**F**, computed from the entire set of simulations with varied initial stimulation. For individual neurons these preferred subthreshold membrane potentials are known as "up" and "down" states [71], and in the context of the ensemble of neurons it seems natural to view these two states as collective "up" and "down", respectively. As seen in Fig 3 **A-E**, a typical period of oscillations is close to 100 ms ($f \approx 10$ Hz).

For a typical neuron in the ensemble, Figs 3 **D-E** illustrate the temporal evolution of the voltage and the membrane recovery variable, respectively, during the same simulation. There is strong correlation between firing of this neuron and the periods of high activity of the whole network, although some other neurons also fire when the network activity is low. These latter are inhibited during the high activity epochs and become disinhibited when the overall network activity is low. We have shown elsewhere the importance of this disinhibitory effect to sustain the long-lived activity of the network in the oscillatory situation [35].

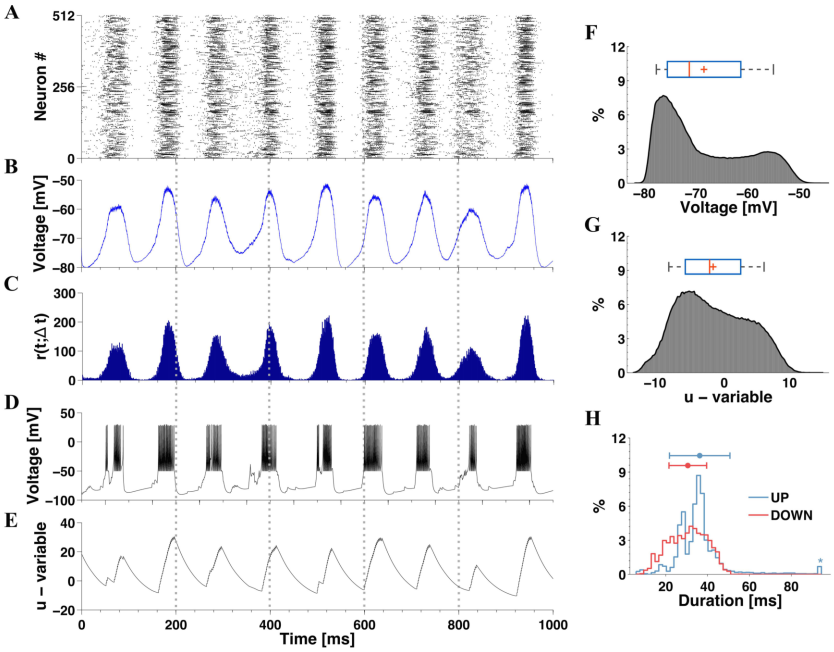

Fig 3. Up and down network oscillations in the noiseless case when inhibition is stronger than excitation. The network is composed of 16%CH, 64%RS and 20%LTS neurons, and $(g_{\text{ex}}, g_{\text{in}}) = (0.15, 1)$. Panels **A-C** show the raster plot for half of the neurons in the network, average voltage and time-dependent firing rate from a sample simulation with long-lived self-sustained activity. Panels **D-E** show the voltage v and membrane recovery variable u extracted from a sample neuron in this simulation. Histograms **F-G** show the distributions of average v and average u based on data from all long-lived simulations. In the box plots above the histograms the red lines and the pluses denote, respectively, the median and the mean. Histogram **H** presents the distribution of stay duration in the collective up and down states based on all simulations, as well as mean and standard deviation; the outlier is indicated by the star in the end of the distribution.

Remarkably, not only the voltage series in Fig 3 **D** features two different states (a hyperpolarized one and a depolarized one) but also the membrane recovery variable, which clearly grows when the network activity is high and slowly relaxes when the network activity is low. This is a global phenomenon: in all simulations there are peaks of the variable u. In the distribution shown in Fig 3 **G**, the maximum is broad due to the time-scale separation of the variables: u is slower than v and its relaxation takes much longer. In [35] we have shown the importance of the recovery variable for the breakdown of global high-activity epochs, which produces the up and down oscillatory pattern.

Fig 3 **H** presents a histogram of durations in collective up and down states. The term "up" refers here to different states in which the network activity is above 20% of its average value, whilst the voltage for the majority of neurons is at a depolarized value. A collective "down" state is identified whenever the bulk of the neurons reaches a hyperpolarized state close to -80 mV.

Recall that eventually the system ceases to oscillate, and voltages of all neurons invariably converge to the rest value.

3.2 Setup with synaptic noise

Introduction of synaptic noise drastically changes one important aspect, both in the individual and in the collective dynamics: the state of rest, albeit formally stable, ceases to be the ultimate attractor. A neuron is an excitable system, and in the noisy setup it is just a matter of time when a sufficiently strong fluctuation (or a cumulative effect of many fluctuations) drives it across the spiking threshold. For an ensemble this implies disordered sporadic firing of its members, which, under favorable conditions, can turn into ordered collective activity. If deterministic aspects dominate in dynamics, this activity will temporarily end in the state of rest, only to be recreated by new fluctuations.

3.2.1 Isolated neurons

Consider an individual neuron that obeys Eq.(1) with the synaptic current I given by Eq.(3) and synaptic conductances $G^{\mathrm{ex/in}}$ obeying Eq.(4) with noisy input. Take the initial conditions for the neuron at its state of rest and set its synaptic conductances to zero, so that the initial current is absent. As time goes on, the conductance evolves stochastically; to ensure that it stays positive, we impose a reflecting condition at zero. As a result, a stochastic current $I(t)$ is generated. As long as $I(t)$ is absent or sufficiently small, the neuron stays at rest. As soon as the instantaneous current I exceeds the critical value $I_{\mathrm{crit}}(t) = \dfrac{(\beta - b)^2}{4\alpha} - \gamma$, with α, β, γ, b being the parameters of the Izhikevich model (1), the state of rest disappears (the mechanism is explained below in Sect. 3.4), the voltage variable v starts to grow monotonically, and the neuron fires.

This description turns the computation of the first firing time for an isolated neuron into a variant of the mean first passage time problem [72] for the Ornstein-Uhlenbeck process. Numerically, we find this quantity by averaging over a sufficient number of trials.

Among the four parameters (a, b, c, d), which define the electrophysiological classes of the Izhikevich neurons, only the parameter b matters in this context: it determines the current threshold value. Three of the four considered neuronal classes share the same value of b, whereas the LTS neuron has a higher value of b, ensuring early initiation of spikes. Hence, it suffices to compare two neurons: LTS and e.g. RS. In Fig 4 we plot the computed dependences of the time of first spike on the synaptic noise intensity.

Notably, from the point of view of the random network, each curve in Fig 4 shows the behavior for all neurons of its respective kind, regardless of their in-degree: according to Eq.(4), an increase of the in-degree (in other words, of the number of independent Gaussian noises acting upon the synapse) rescales the variance and is therefore equivalent to the corresponding increase of D at constant degree. Recall that in the studied networks most of the neurons have in-degree ≈ 10. Altogether, the influence of the number of synaptic connections is clear: the higher the in-degree, the higher the variance of the input noise and the faster the neuron crosses the threshold and emits a spike.

3.2.2 Network with weak synaptic noise

We begin the discussion of synaptic noise in the network by presenting a case where its introduction induces activity with properties strongly different from those in the deterministic setup. For the same set of parameter values as in the deterministic case of Fig 3, instead of initial stimuli, we add in accordance with Eq.(4) small ($D = 2.5 \times 10^{-6}$) stochastic fluctuations to the synaptic variables. This results in activity with very low firing rates, exemplified in panels **A-C** of Fig 5. The high spectral entropy ($H_s = 0.82$) and the very low synchrony index ($\Sigma = 2 \times 10^{-4}$) indicate

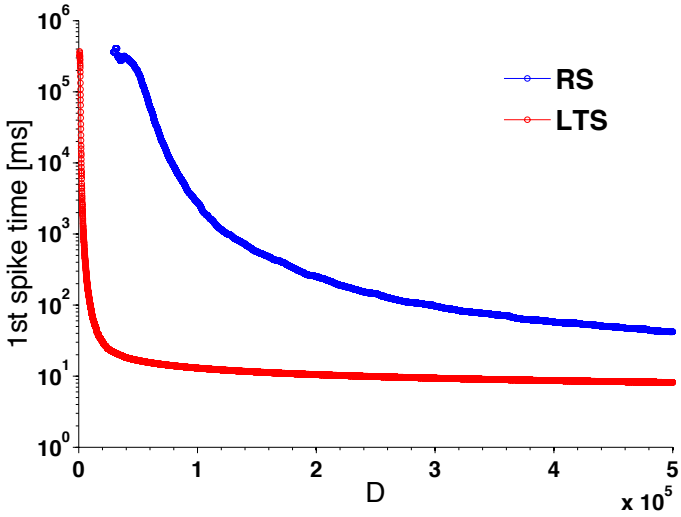

Fig 4. Average time of first spike for the Izhikevich neuron model driven by synaptic noise. D: noise intensity. Blue curve: RS neuron. Red curve: LTS neuron.

a non-oscillatory and asynchronous type of activity. The voltage distribution in Fig 5 **D** stands in contrast to the deterministic case: it is unimodal, the maximum lies at the mean, and the relevant voltage values are close to the resting potential. The firing rates in Fig 5 **E** are close either to 1 Hz (excitatory neurons) or to 8 Hz (inhibitory neurons). The distribution of interspike intervals features exponential decay, typical of cortical neurons [77]. The state of the network in the weak synaptic noise setup corresponds well to the so-called asynchronous irregular (AI) state [21, 29].

Up-down oscillations can be seen in the weak synaptic noise setup, but only for short transient periods like in the deterministic setup. After the transient, the persistent activity is asynchronous irregular like the one in Fig 5. An example is shown in S1 Fig.

3.3 Onset and classification of intermittent oscillatory and quiescent activity in the synaptic noise setup

Here we describe various collective states induced in the network by synaptic noise. Experience gained from the study of the deterministic setup allows us to expect that, along with the synaptic noise intensity D, the crucial parameter in this context is the ratio $g_{\text{in}}/g_{\text{ex}}$: the proportion between inhibition and excitation [21, 57]. We start by exploring the behavior of the spectral entropy H_s and the synchrony index Σ in the two-dimensional diagram spanned by parameters $g_{\text{in}}/g_{\text{ex}}$ and D (Fig 6).

As shown in the diagrams in Fig 6, both $g_{\text{in}}/g_{\text{ex}}$ and D are responsible for shaping the activity pattern of the network. Let us first consider the diagram for spectral entropy in Fig 6 **A**. For weak synaptic noise ($D \lessapprox 5 \times 10^{-6}$) the network displays non-oscillatory behavior independently of the $g_{\text{in}}/g_{\text{ex}}$ ratio. For the narrow horizontal band defined by $5 \times 10^{-6} \lessapprox D \lessapprox 10^{-5}$, the state of the network is oscillatory and the degree of oscillatory activity is higher for $g_{\text{in}}/g_{\text{ex}} \lessapprox 2$ (corresponding to the excitation-dominated region). On the other hand, for $D \gtrapprox 10^{-5}$ the situation is inverted and the region determined by $g_{\text{in}}/g_{\text{ex}} \lessapprox 2$ displays non-oscillatory activity while most of the remainder of the diagram displays oscillatory activity. Within this latter part of the diagram, increase of both noise and inhibitory strength lowers the degree of oscillatory activity until in the upper right corner the activity becomes non-oscillatory.

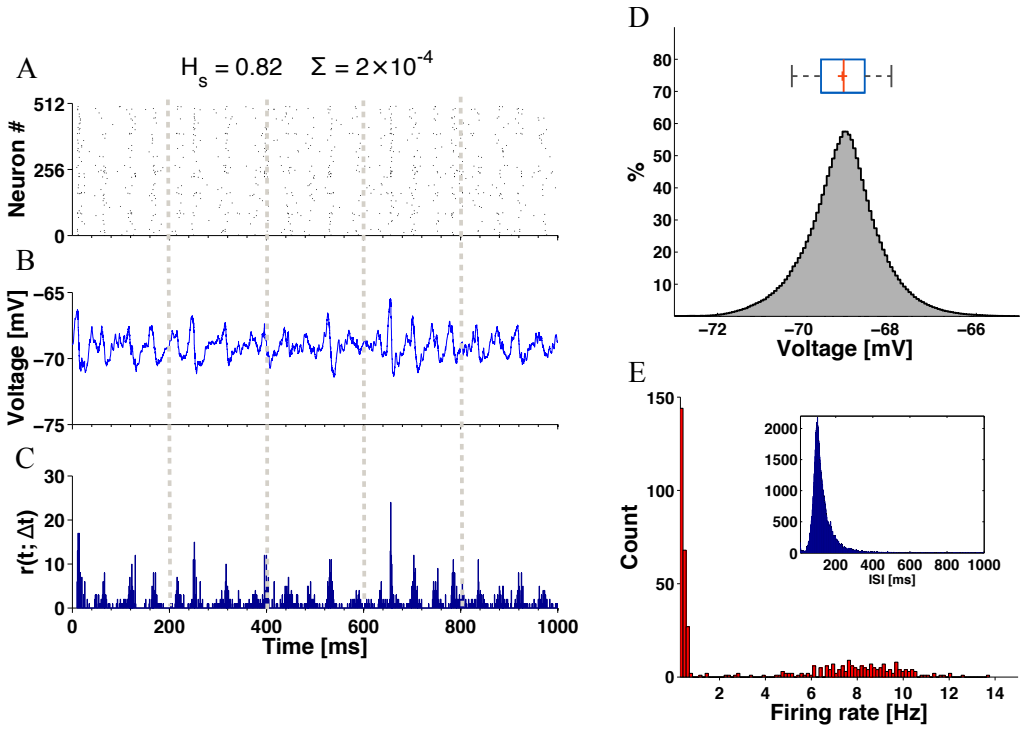

Fig 5. Asynchronous irregular state in the presence of weak synaptic noise. The network, composed of 16%CH, 64%RS and 20%LTS neurons, evolves without initial stimulation. Synaptic increments: $(g_{\rm ex}, g_{\rm in}) = (0.15, 1)$. Intensity of synaptic noise: $D = 2.5 \times 10^{-6}$. Panels **A-C** present, respectively, raster plot for half of the neurons in the network, average voltage and time-dependent firing rate for the network. Above them are given the values of H_s and Σ. Panels **D-E** are histograms with distributions of average voltage and firing rates. The inset in **E** shows the interspike interval (ISI) distribution for the ensemble of neurons in the network.

Let us now consider the diagram for synchrony index in Fig 6 **B**. The weak synaptic noise region ($D \lessapprox 5 \times 10^{-6}$) displays asynchronous behavior independently of the $g_{\rm in}/g_{\rm ex}$ value. Under such weak noise firing remains an individual property of noise-perturbed neurons, rather than a collective effect. Along the narrow horizontal band of the diagram determined by $5 \times 10^{-6} \lessapprox D \lessapprox 10^{-5}$, the synchrony index changes from relatively high for $g_{\rm in}/g_{\rm ex} \lessapprox 3$ to low when $3 \lessapprox g_{\rm in}/g_{\rm ex} \lessapprox 5.5$ to zero when $g_{\rm in}/g_{\rm ex} \gtrapprox 5.5$; in other words, along this narrow noise intensity interval synchrony decreases as the relative strength of inhibition increases. In the remainder of the diagram, until $D \approxeq 10^{-3}$, the behavior along horizontal scans in the diagram is roughly the same: in the entire region determined by $g_{\rm in}/g_{\rm ex} \lessapprox 3$ the activity is highly synchronous, whereas outside that region the degree of synchrony decreases when $g_{\rm in}/g_{\rm ex}$ grows, and turns almost zero for inhibition much greater than excitation. In the upper part of the diagram, for high D values above 10^{-3}, the situation is similar to the last one but now the synchrony index decreases not to zero but to finite low values when inhibition grows.

The combined information in the two diagrams of Fig 6 can be qualitatively represented in a schematic diagram drawn in Fig 7. The terminology used to describe states in this diagram is based on the meaning of the two measures we used to characterize network activity in Fig 6: H_s quantifies the degree of oscillatory activity and Σ quantifies the degree of synchrony.

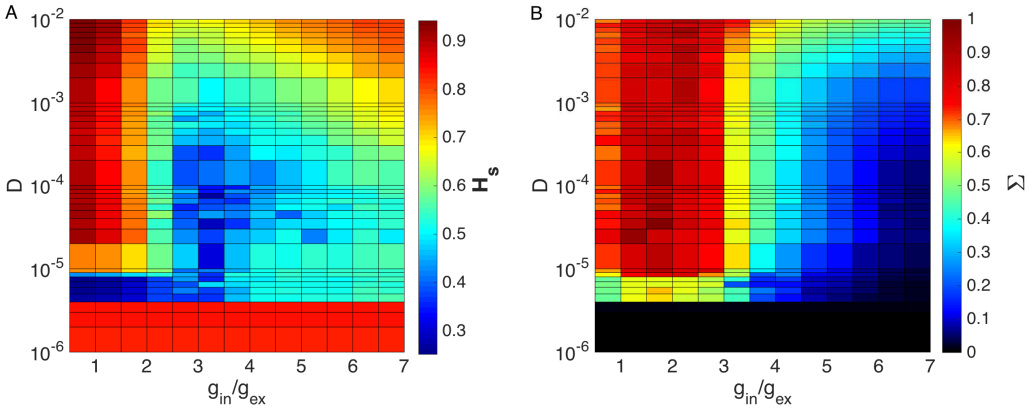

Fig 6. Spectral entropy and synchrony index for the synaptic noise setup. Two-dimensional space where ordinate represents the synaptic noise intensity D and abscissa, the ratio of synaptic increments $g_{\mathrm{in}}/g_{\mathrm{ex}}$. The coordinate mesh is linear (from 0.5 to 7) with respect to $g_{\mathrm{in}}/g_{\mathrm{ex}}$ and logarithmic with respect to the synaptic noise intensity (from $D = 1 \times 10^{-6}$ to $D = 1 \times 10^{-2}$). Panel **A**: Colors represent spectral entropy H_s (values close to zero correspond to oscillatory states and values close to 1 correspond to non-oscillatory states). Panel **B**: Colors represent synchrony index Σ (values close to zero correspond to asynchronous states and higher values correspond to states with increasing degrees of synchrony).

At the bottom of the diagram in Fig 7 there is the region of weak synaptic noise. The type of network activity there is asynchronous non-oscillatory, already described in subsection 3.2.2. It is similar to the asynchronous irregular (AI) activity observed in networks of LIF neurons [21, 29]. The region stretches along the full length of the horizontal axis, indicating that the generic features of the network activity for weak synaptic noise are insensitive to the ratio between excitation and inhibition.

For stronger synaptic noise the structure of the diagram in Fig 7 is more complex. The network displays synchronous oscillatory activity within an irregular-shaped region in the center of the diagram, adjoined by a narrow horizontal strip in the bottom part. This is similar to the synchronous regular (SR) type of activity found in networks of LIF neurons [21, 29]. In the remainder of the excitation-dominated region of the diagram (roughly the third of the diagram) beyond the mentioned narrow horizontal stripe and for the whole upper part of the diagram well into the range of high g_{in}/g_{ex}, the activity is synchronous and non-oscillatory. Its pattern is similar to the constant pattern shown in the left column of Fig 2. Thus, in the same fashion as for weak synaptic noise, for very strong synaptic noise the generic features of the network activity are insensitive to the ratio between excitation and inhibition.

Finally, the diagram in Fig 7 includes the region marked as "transition". It contains most of the right third of the diagram, with the exception of the regions of weak and strong synaptic noise mentioned above, and extends to the central part of the diagram where it separates the synchronous oscillatory from the synchronous non-oscillatory regions. This corresponds to a region with intermediate degrees of oscillatory activity (the greenish region in the diagram for H_s in Fig 6 **A**), and a range of synchrony levels which vary from low to middle (dark to light blue colors) in its right-hand half to middle to high (green to red) in its left-hand half. Because of this, states in the transition region are expected to have intermediate features between constant and oscillatory states like the state in the middle column of Fig 2.

Interested in the behavior of the network in the transition region, we focus here on a

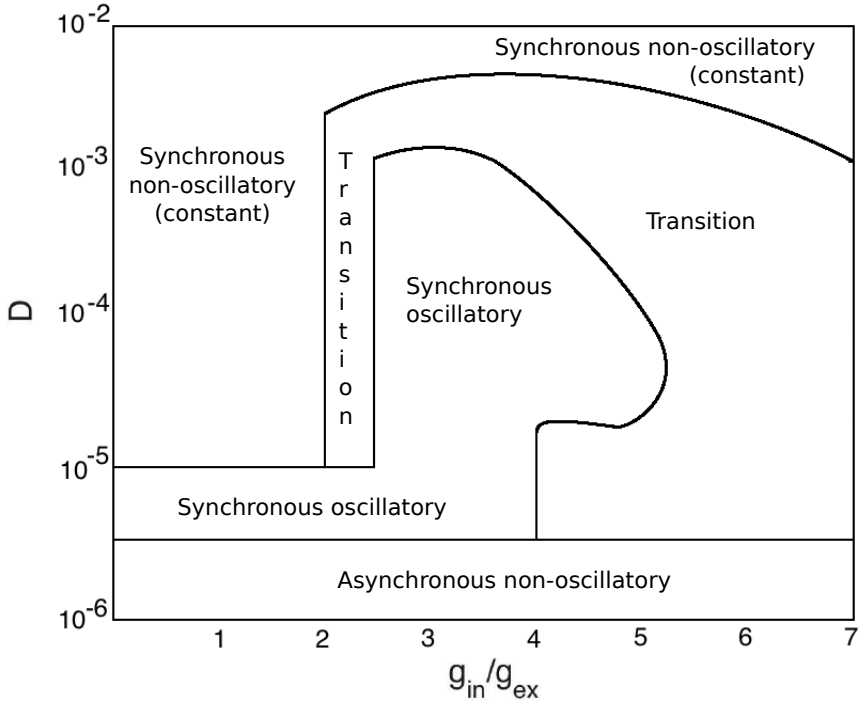

Fig 7. Network activity patterns in the synaptic noise setup. A schematic representation of the D vs. $g_{\text{in}}/g_{\text{ex}}$ diagram of Fig 6 combining the information on degree of oscillatory activity (H_s) and degree of synchrony (Σ) disclosed in that figure. The names of the activity types are given inside the regions bounded by full lines. The synchronous non-oscillatory type is equivalent to the constant type used to describe network states in the deterministic setup. The region marked as "transition" corresponds to states with intermediate levels of oscillatory activity and synchrony.

region of the diagram in Fig 7 determined by $(g_{in}, g_{ex}) = (1, 0.15)$, which implies $g_{in}/g_{ex} \approx 6.66$, and $10^{-5} \lessapprox D \lessapprox 10^{-4}$. This corresponds to the greenish (dark blue) region on the lower right-hand side of the diagram for H_s (Σ) in Fig 6 **A** (**B**). The spectral entropy here is close to 0.5 and the synchrony index is close to 0.1 meaning that both oscillatory and non-oscillatory states at a low synchrony degree may be encountered.

We illustrate the behavior in this region of the diagram in Fig 8. The network is the same used to generate Figs. 3 and 5.

Remarkably, a typical record of a long simulation trial in this region of the diagram consists of alternating states (Fig 8): an oscillatory one, akin to oscillations presented in the deterministic setup in Fig 3, and a state with very low firing rates similar to the one in Fig 5. From time to time transitions between these states occur, seemingly without any precursors. Compared to deterministic simulations, an additional feature is distinct in the histogram of mean voltage: a pronounced maximum at the state of rest. Accordingly, the temporal evolution of the voltage is organized around three characteristic values instead of two as in the deterministic setup. Three red dashed lines in Figs 8 **B-C** mark these three relevant states; from top to bottom, they denote depolarization, the state of rest and hyperpolarization. Note that the histogram in **B** can be viewed as a combination of the voltage histograms from Figs 3 and 5.

The average spectral entropy calculated over the quiescent/oscillatory states in Fig 8 is $H_s = 0.74/H_s = 0.37$, indicating non-oscillatory activity in the first case and oscillatory activity in the second one. To estimate the synchrony index for the quiescent/oscillatory states using the time window of $T = 2000$ ms defined in Sect. 2.2, we cropped and glued the raster plot to create versions containing merged pieces of exclusively oscillatory/quiescent states. The calculated synchrony indices are $\Sigma = 8 \times 10^{-4}$ for the raster plot containing only quiescent periods, indicating asynchronous activity, and $\Sigma = 0.20$ for the raster plot containing only oscillatory periods, indicating synchronous activity.

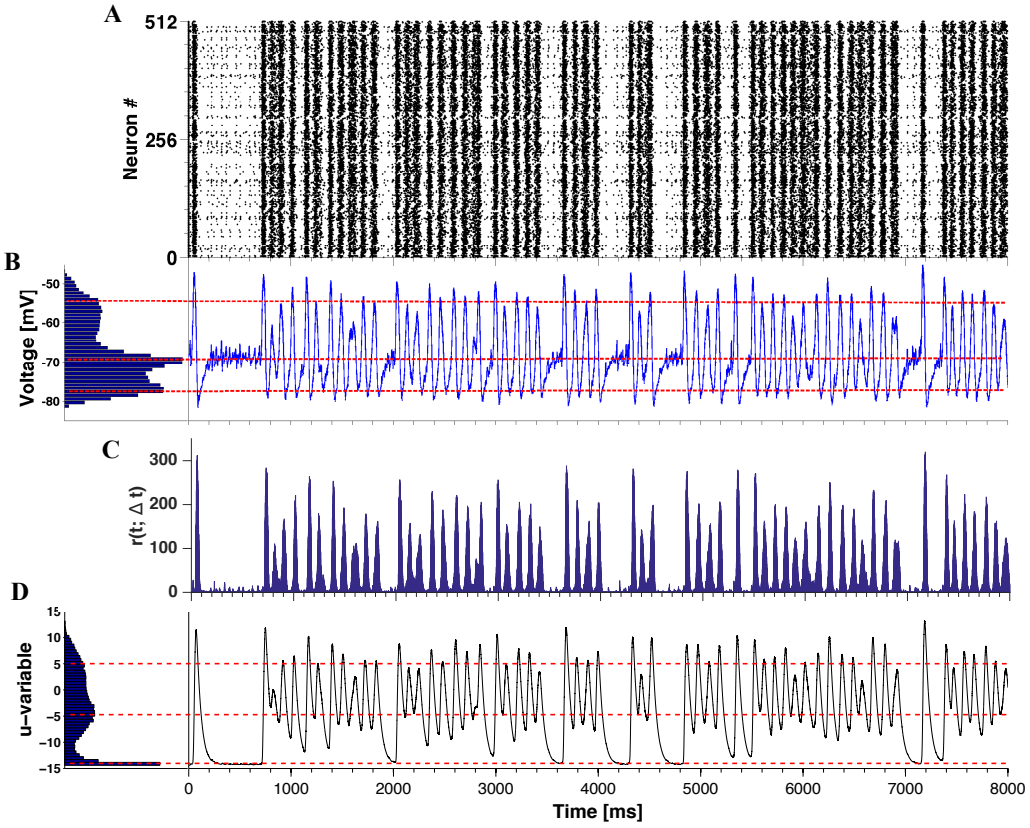

Fig 8. Intermittent transitions between active oscillatory and quiescent regimes in the presence of synaptic noise. Plots generated for a network with 16%CH, 64%RS and 20%LTS neurons, $D = 1 \times 10^{-5}$ and $(g_{in}, g_{ex}) = (1, 0.15)$. Panel **A**: Raster plot for half of the neurons in the network. Panel **B**: voltage v histogram (left) and time course of average voltage over all network neurons (right). Panel **C**: time-dependent firing rate of the network. Panel **D**: Recovery variable u histogram (left) and time course of average recovery value over all network neurons.

We classify the observed states based on two attributes: network activity and average voltage. Like previously, the average voltage series was used to detect the up and down states (see Fig 3 **H**). The states close to rest are identified through very low network activity,

In terms of activity, we introduce the following distinction:

- **quiescent period** is the time interval when the time-dependent firing rate of the network $r(t, \Delta t)$ is below its maximum by at least 20%, and most of the single

neurons have voltage values close to the resting state. During a quiescent period there can be sporadic noise-induced spikes but no collective dynamics. The state is similar to an asynchronous irregular (AI) state of networks of LIF neurons [21, 22] with low firing rate, and to a desynchronized cortical state as described in the Introduction.

- **active period** is the time interval when the network exhibits oscillatory activity, alternating between high depolarized and hyperpolarized mean voltage values: collective up and down states. Such behavior can be related to the self-sustained activity developed in *in vivo* cortical slice preparations and during slow-wave sleep and anesthesia [10, 13, 35].

These definitions, in combination with the values of the average voltage, facilitate identification of different collective states. Certain states that look very similar on the raster plot turn out to differ in typical voltage values. For instance, both the down state and the quiescent period feature in the raster plot almost no activity, but can be easily distinguished in terms of the average voltage.

In Fig 9 we show various regimes at different values of D. Three samples corresponding to the time interval of 2 s are, from top to bottom: $D = 0.5 \times 10^{-5}$, $D = 1.5 \times 10^{-5}$, and $D = 4.5 \times 10^{-5}$, respectively. In panels **A1**, **B1**, and **C1** green dots denote states with instantaneous voltage values close to the resting state, blue dots denote hyperpolarized voltage (down state), and red dots denote depolarized voltage (up state). The plot highlights the crucial role of synaptic noise level in changes of typical duration at each of these states. It is easier to generate oscillatory states (alternating between up and down states) when the network is subjected to stronger synaptic noise. In contrast, the "green" states close to rest (quiescent periods), prevalent at low synaptic noise amplitudes, occupy a much smaller proportion of time when synaptic noise becomes sufficiently intensive.

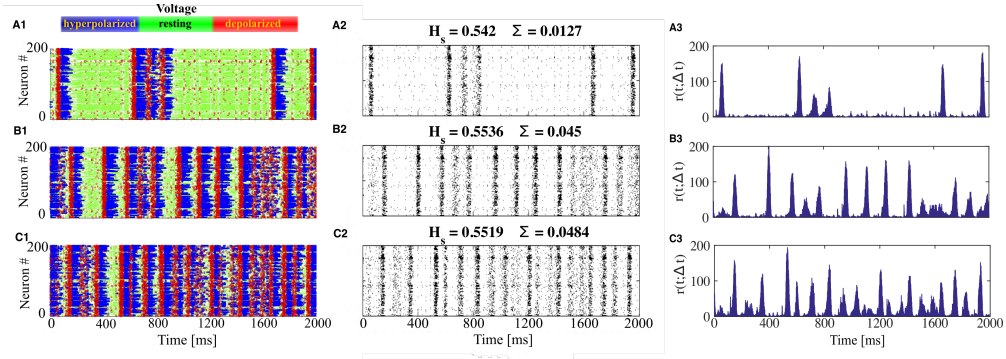

Fig 9. Increase of synaptic noise favors up-down oscillations. The network has the same composition as in Fig 8 with varying synaptic noise intensity D. **A**: $D = 0.5 \times 10^{-5}$, **B**: $D = 1.5 \times 10^{-5}$, **C**: $D = 4.5 \times 10^{-5}$. In **A1**, **B1**, and **C1** blue dots correspond to depolarization (up state), red dots to hyperpolarization (down state), and green dots to voltage near the resting state. **A2**, **B2**, and **C2**: raster plots for 200 neurons in the network with corresponding H_s and Σ values atop each plot. **A3**, **B3**, and **C3**: time-dependent firing rates.

Comparison of raster plots in Fig 9 indicates that when noise intensity D is increased, the waves of activity start to merge. This hinders identification of states, based on the raster plot alone. The spectral entropy and the synchrony index increase with the noise intensity. We expect that at very high levels of noise the activity becomes constant (synchronous non-oscillatory), with rather high firing frequencies (see the schematic diagram in Fig 7).

In the frequency domain, variation of the noise level leads to redistribution of power in the Fourier spectra of both the spike trains and the voltage series. Fig 10 presents spectra for the same noise intensities as in Fig 9: from top to bottom, $D = 0.5 \times 10^{-5}$, $D = 1.5 \times 10^{-5}$, and $D = 4.5 \times 10^{-5}$. All spectra were averaged over ensembles of 200 neurons, see equation 7. The shapes of spectral curves for spike trains and for voltage values are similar; the only noticeable difference is the somewhat faster decay at high frequencies in the voltage spectra. The left column shows mixtures of RS and LTS neurons; the right column corresponds to networks with RS and FS neurons. At low levels of noise, spectral power is concentrated at very low frequencies, waves of collective activity are quite rare and, when they occur, they are mostly isolated events. On increasing the intensity D, waves of collective activity become more frequent whereas the periods of quiescence get shorter. During the periods of oscillatory activity, neurons are either firing at high frequency in the up state or rarely firing in the down state. This results in the increase of spectral power at low frequencies, with a distinct maximum near 10 Hz.

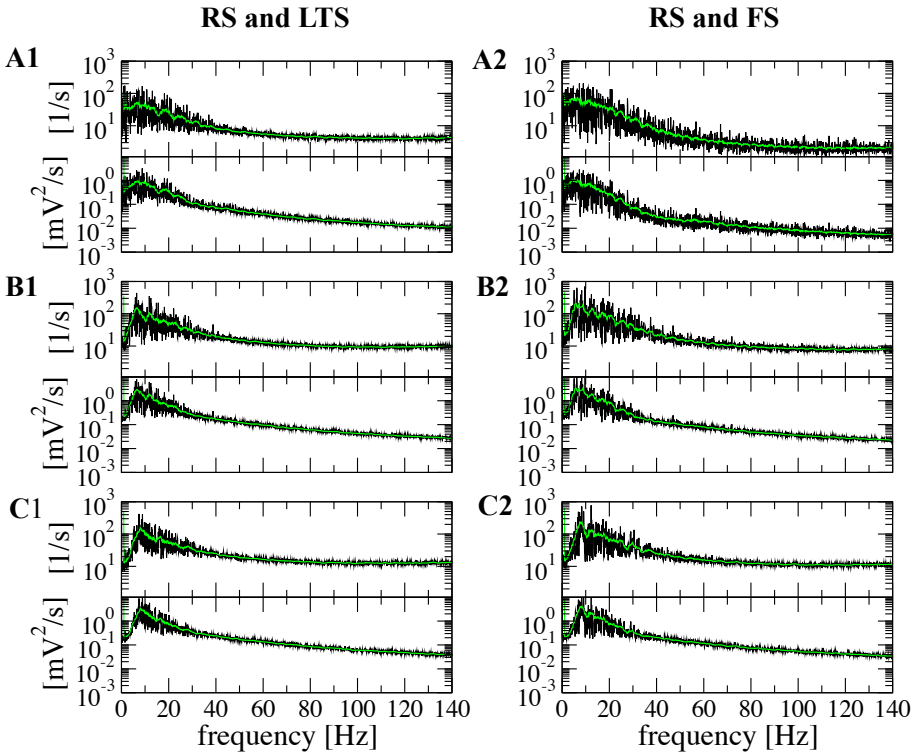

Fig 10. Averaged power spectra at different noise intensities. Simulation length: 10 s. Left column: network with inhibitory LTS neurons. Right column: network with inhibitory FS neurons. Noise intensities: **A**: $D = 0.5 \times 10^{-5}$, **B**: $D = 1.5 \times 10^{-5}$, **C**: $D = 4.5 \times 10^{-5}$. Black curves in upper subpanels: averaged spectra of spike trains for 200 randomly chosen neurons. Black curves in lower subpanels: averaged spectra of voltage for the same 200 neurons. Green curves: moving average over 20 points.

Comparison of left and right columns in Fig 10 shows that spectral curves for networks with inhibitory LTS and FS neurons are similar. Spectral power in the networks with FS neurons is slightly higher.

Remarkably, these power spectra, computed for single neurons, bear resemblance to

experimentally obtained spectral curves [69].

We have seen that synaptic noise enforces alternation of collective states and influences durations of stay in each of them. Below, we explain how the dynamics of a single neuron, embedded in the synaptic noise setup, is reflected in the collective properties of activity, how the transitions are affected by the composition of the network, and how the picture changes at different levels of noise.

3.4 Single neuron phase plane description of the synaptic noise setup

A deeper understanding of the single neuron behavior in the synaptic noise setup can be gained from analysis of the course of its phase plane dynamics during the simulation. Setting the derivatives $\dot{v}$ and $\dot{u}$ in Eq.(1) to zero renders the nullclines of the voltage and the membrane recovery variable which we denote below as $\bar{u}$ and u^*, respectively.

$$\begin{cases} u &= \bar{u} = \alpha v^2 + \beta v + \gamma + I(t), \\ u &= u^* = bv. \end{cases} \tag{11}$$

with $\bar{u}$ being a (time-dependent) quadratic parabola and u^* a straight line. Synaptic noise enters this configuration implicitly, through its contribution to the current I.

Under the employed values of the parameters (see Table 1 above) and $I = 0$, the nullclines intersect in two points of the phase plane. These points correspond to equlibria of the system; the left of them is stable: without input current, neuron shows no activity. When the instantaneous value of the current is increased, the nullcline $\bar{u}$ is shifted upwards on the phase plane, and the equilibria move towards each other. At the critical value $I_{\mathrm{crit}}(t) = \dfrac{(\beta - b)^2}{4\alpha} - \gamma$ they merge and disappear in the course of a saddle-node bifurcation. This is the minimal current that is required in order to ignite a spike: in absence of equilibria, the voltage grows until it reaches the threshold.

Evolution of every individual neuron is governed by its instantaneous location on the phase plane with respect to the nullclines; its dynamics is affected not only by its own state, but by the time-dependent (due to external and synaptic currents) position of the nullcline $\bar{u}$. This gives us a possibility to see the collective dynamics from the local point of view of its individual participant; for it, the rest of the network is a background mechanism that moves the nullcline $\bar{u}$ upwards and downwards.

With this local view in mind, we present in Fig 11 the same simulation as in Fig 8 focusing on the evolution of one arbitrarily picked neuron (neuron # 240), which fires only during the active periods, in the time range between 3800 ms and 4400 ms. We split this time range, which contains both active and quiescent states, into 6 smaller intervals Δt_i, each one of 100 ms duration. The upper panel in Fig 11 shows the entire time range and its breakdown into the set of Δt_i. The lower panels present for every Δt_i the voltage series and the trajectory on the phase plane. Notably, in the hyperpolarized (down) state below reset, the neuron typically is close to the instantaneous location of $\bar{u}$, hence its motion is slow.

We summarize our observations as follows:

- Interval Δt_1: in the beginning, the neuron has just ended its evolution in an up state and passes through a down state (dashed red line). There, the trajectory mostly stays inside the parabola of the voltage nullcline $\bar{u}$ below the reset value. Since the system is located above the recovery variable nullcline u^*, the latter decreases. The down state can be viewed as a period of relaxation where the voltage is hyperpolarized. The trajectory slowly moves towards the state of rest, but before it arrives there the neuron receives excitatory input from its presynaptic partners, resumes the up state and fires several times.

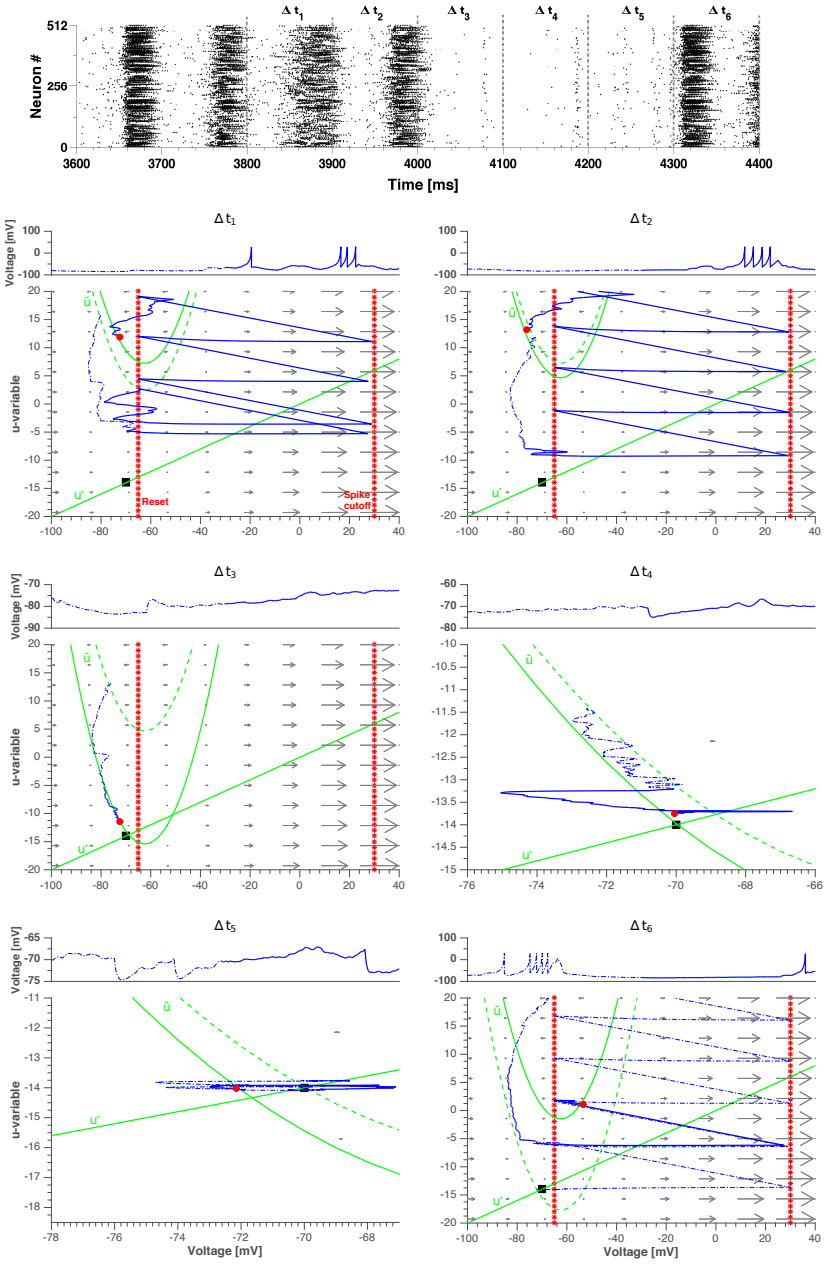

Fig 11. Single neuron phase plane depiction of a neuron that fires during the *active* periods in the synaptic noise setup. Upper panel: a zoom of the simulation from Fig 8, split into 6 time intervals Δt_i with duration 100 ms. Lower panels: voltage series and dynamics on the phase plane of neuron # 240 in subsequent intervals Δt_i. Blue dashed line: the first 50 ms of evolution. Blue solid line: the last 50 ms of evolution. Red circle: location of the neuron at the end of the time interval. Black square: location of the state of rest with $v = v_{\text{rest}}$ and $u = u_{\text{rest}}$. Dotted red lines: reset value of voltage and spike cutoff. Green lines: Nullclines $\bar{u}$ and u^*, according to Eq.(11). The location of the parabolic nullcline $\bar{u}$ is time-dependent; its position at the beginning (respectively, end) of Δt_i is shown with dashed (respectively, solid) green line.

- Interval Δt_2: the behavior is largely similar to the interval Δt_1. During the active period this kind of behavior is roughly repeated every ≈ 100 ms. Frequent synaptic input keeps the nullcline $\bar{u}$ in a high position, opening possibilities for repeated firing.

- Interval Δt_3: the network does not provide synaptic input, and the conductances $G^{ex/in}$ relax. As a result, the nullcline $\bar{u}$ lowers and the neuron approaches the state of rest.

- Interval Δt_4: This is the middle of a quiescent period. The zoomed image shows how the neuron slowly approaches the state of rest. The membrane recovery variable u monotonically decays. Synaptic noise perturbs the trajectory, but falls short of initiating a new up state.

- Interval Δt_5: the neuron crosses the nullcline u^* of the recovery variable u. The latter does not decrease anymore while the voltage is fluctuating due to noisy synaptic input.

- Interval Δt_6: finally the noise and/or arrival of inputs from presynaptic neurons are able to initiate a new active period.

The sequence of events in Fig 11 discloses a major role of the membrane recovery variable u both in the transition from up state to down state and in the subsequent initiation of the new active phase by the noisy input. Because of high tonic firing during an up state, the total synaptic current into a neuron like the one in Fig 11 is very intense and roughly constant (its fluctuation amplitude depends on the synaptic noise level). Hence, the nullcline $\bar{u}$ stays at its highest position in the u-v diagram while the neuron climbs towards it due to the increments received by its recovery variable u after each spike. Eventually, the neuron gets inside the parabolic nullcline $\bar{u}$ and stops firing. The fact that the whole network enters a down state when this happens suggests that most neurons behave like this neuron, i.e. they dominate dynamics in the network. The excursion of the neuron to the left of the reset line while it is inside the parabola $\bar{u}$ is the mechanism responsible for the hyperpolarized voltages seen in the down states of oscillatory regimes both in the deterministic (cf. Fig 2) and noisy (cf. Fig 8) setups. During a quiescent period, the nullcline $\bar{u}$ is dragged to the bottom of the diagram putting the neuron close to rest. This explains the absence of hyperpolarized voltages during quiescent periods (cf. Fig 8). In this situation the neuron is also close to the nullcline u^*, so an eventual high jump of the neuron to the region of the diagram below the nullcline u^* makes the neuron fire again and a new active period begins.

The behavior of the neuron in Fig 11 somewhat mimics the overall behavior of the network: it is highly active during up states of active periods and silent during down states of active periods and quiescent periods. In the following, we will refer to neurons of this type as "typical" in the sense that they represent the behavior of the majority of the network nodes.

To complete the single neuron phase plane view on global network dynamics, in Fig 12 we show the behavior of a second neuron (neuron # 69) chosen because of its atypical behavior: it fires at all stages: in the up and down states of the active period and during the quiescent period. The features of the behavior of this second neuron (Fig 12) are complementary to the ones of the typical neuron in Fig 11, and a combination of the views given by them offers a deeper understanding of the mechanisms responsible for the intermittent changes between active and quiescent states.

A summary of our observations for the neuron in Fig 12 is given below:

- Interval Δt_1: contrary to the typical neuron, # 69 starts its evolution with a low value of the recovery variable u. The nullcline $\bar{u}$ also begins this time interval at a

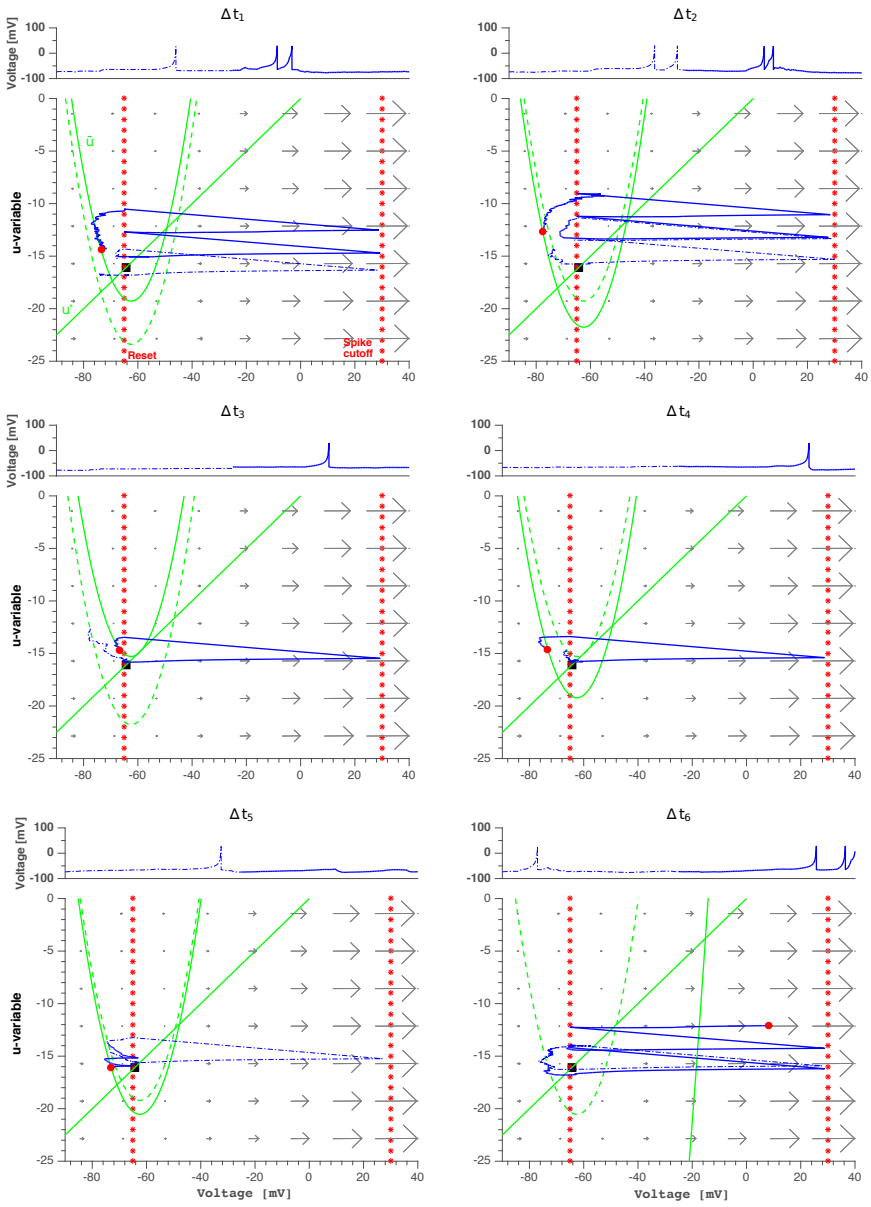

Fig 12. Single neuron phase plane depiction of a neuron that fires during *all* periods in the synaptic noise setup. Each panel contains voltage series and dynamics on the phase plane of neuron # 69 for the same time range (3800–4400 ms) and the same six time intervals of 100 ms as for the neuron in Fig 11. Blue dashed line: the first 50 ms of evolution. Blue solid line: the last 50 ms of evolution. Red circle: location of the neuron at the end of the time interval. Black square: location of the state of rest with $v = v_{\text{rest}}$ and $u = u_{\text{rest}}$. Dotted red lines: reset value of voltage and spike cutoff. Green lines: Nullclines $\bar{u}$ and u^*, according to Eq (11). The location of the parabolic nullcline $\bar{u}$ is time-dependent; its position at the beginning (respectively, end) of Δt_i is shown with dashed (respectively, solid) green line.

low position. This means that during the previous up state the neuron did not fire much: its nullcline $\bar{u}$ did not receive many increments. This suggests that the neuron is heavily inhibited when the network is at a high firing state, possibly

being postsynaptic to a large pool of inhibitory neurons. Then, it is more likely that the neuron emits spikes during down states because at such states it receives less inhibition from its presynaptic neurons, which, like the typical neuron in Fig 11, are relaxing toward rest. Due to synaptic noise or eventual inputs from other neurons in a similar situation, the neuron fires at a low rate during the down state (first half of the time interval). When the network enters the up state (second half of the time interval), the neuron is again strongly inhibited and emits fewer spikes than a typical neuron.

- Interval Δt_2: the behavior is largely similar to the one in interval Δt_1.
- Interval Δt_3: the network enters a quiescent period. Differently from the nullcline $\bar{u}$ of the typical neuron, which moves down when a quiescent period begins, the nullcline $\bar{u}$ of this neuron is already at a low position because of its weak firing in the previous up state. Hence, the neuron approaches the state of rest much faster than the typical neuron. Even weak synaptic noisy inputs can make the neuron fire. The firing rate depends of the synaptic noise level, and consequently the duration of the quiescent period also depends on it.
- Interval Δt_4: This is the middle of the quiescent period and the situation is largely similar to the previous one. Notice that the nullcline $\bar{u}$ has moved down by the end of the time interval, indicating a net inhibitory input to the neuron (an early sign of the recovery of network activity which will come in the next time steps).
- Interval Δt_5: The situation is still as in the last time interval, but now we can see a clear sign of the strong inhibition received by the neuron. After a spike in the first half of the time interval, when it is close to emitting a new spike, the neuron receives a strong inhibitory kick which hyperpolarizes its voltage and prevents the spike. The voltage grows again but another strong inhibitory kick once more hyperpolarizes the neuron. These inhibitory inputs come from neurons in the pool of inhibitory presynaptic neurons to this neuron, which are starting to "wake up" on the eve of a new active period. As a consequence of the inhibitory inputs, the nullcline $\bar{u}$ moves further down.
- Interval Δt_6: The network enters the up state of an active period and most neurons are again active (like the typical neuron in Fig 11). This makes # 69 fire but because of the heavy inhibition, not at a high rate of the typical neuron. Evidence of the strong increase in the inhibitory input received by the neuron comes from the dramatic downward movement of the nullcline $\bar{u}$ out of the scale of the plot.

Neurons like the one in Fig 12, which fire at low rates at all periods, will be called here "quiet" neurons (elsewhere, in the context of the deterministic setup, we called them "moderately active neurons" [35]). Quiet neurons are fewer than typical neurons.

The sequence of events depicted in Fig 12 discloses the importance of inhibition and synaptic noise in shaping the network activity during both down states and quiescent periods. The quiet neurons, which are strongly inhibited during up states, become disinhibited at the end of those states and serve as a source for most of the spikes occurring during down states and quiescent periods. Thus, the firing pattern in the down states and quiescent periods is basically due to the recurrent synaptic connections among quiet neurons, The weak noise limit (cf. Fig 5) discloses the nature of the intrinsic activity pattern generated by the population of quiet neurons: it is highly asynchronous and non-oscillatory; remarkably, it is also weak. This confirms, on the one hand, that the population of quiet neurons is small, and explains, on the other hand,

why the network activity seen during down states and quiescent periods is asynchronous and irregular.

Due to the weakness of their intrinsic activity, the likelihood that the pool of quiet neurons can trigger a high firing (up) state in the network is low and the synaptic noise level plays a pivotal role in controlling this likelihood. At low synaptic noise level, the weak activity of the quiet neurons can restore the up state when the network is at a down state, but this can be repeated generating a sequence of up-down oscillations only for a short transient time. An example can be seen in S1 Fig. After the transient the network enters a quiescent period, which is a persistent low activity regime characterized by asynchronous non-oscillatory activity. When the network is in a quiescent period, the activity of the quiet neurons is too weak to start a high firing state in the network; a certain minimal synaptic noise level is necessary to trigger this state. In the absence of this minimal synaptic noise level, the network activity remains in the quiescent regime as seen in the diagrams of Figs 6 and 7. When the synaptic noise intensity increases above minimum level, the recurrent excitation amongst quiet neurons gets stronger, as well as the synaptic noise inputs to typical neurons, and the probability of the network exiting a quiescent period increases.

The above discussion highlights a fundamental difference between down states and quiescent periods. In the weak synaptic noise regime, when the network activity is dictated by quiet neurons, the weak activity of the latter is able to restore a high firing state in the network when the network is in a down state but not when it is in a quiescent period. This phenomenon bears some similarity with the behavior observed previously by us in deterministic networks of two-dimensional nonlinear integrate-and-fire neurons in the absence of external inputs [34, 35]. There, the network state oscillates for a transient time between up and down states, before decaying to rest (cf. the behavior of the network in the deterministic setup in Sect. 3.1). The decay to rest always occurs when the state of the network in its high-dimensional deterministic phase space passes through a particular region of the phase space (a "hole") which, when represented in the two-dimensional space of average voltage $\langle v \rangle$ and recovery $\langle u \rangle$ variables, overlaps with the region traversed by the network state when it is in a down state [35]. The analogy between down/rest state for the deterministic network without external input and down/quiescent state for the network in the synaptic noise setup suggests a further analogy between the hole in the high-dimensional phase space of the deterministic network and a hole in the high-dimensional phase space of the stochastic network. The difference is that when the network state in the stochastic high-dimensional phase space passes through its corresponding hole it escapes to a quiescent state instead of the resting state, and it can leave this quiescent state when the synaptic noise intensity is above a minimum level.

3.5 Influence of synaptic noise upon different states

Having demonstrated in the previous section that synaptic noise affects different phases of activity, we now proceed to a quantitative description. We compute the average duration of active and quiescent periods in sufficiently long (we take the value of 6×10^5 ms) trials. The mean duration is an important measure to characterize and model alternating states, e.g. in the course of transitions between brain rhythms [14, 53].

Results of simulations confirm that the duration of stay in both active and quiescent periods is affected by the synaptic noise level (Fig 13), but in a twofold way: when the noise intensity grows, active periods elongate whereas quiescent periods shorten. This implies that synaptic noise influences transitions between the states. Remarkably, the average duration of stay in the quiescent state rapidly falls at the increase of small noise amplitude but seems to reach a certain saturation at moderate noise intensities: apparently, the minimal time that the neurons need to organize a new collective activity

is dynamically constrained by the network topology and deterministic characteristic times in the phase space, and in the studied case cannot be made lower than ≈ 80-100 ms.

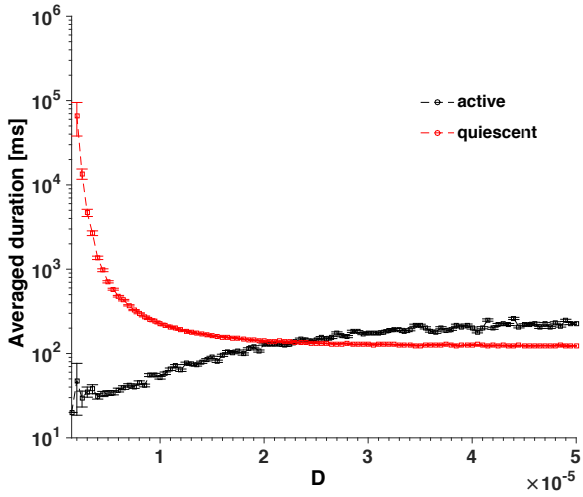

Fig 13. Synaptic noise intensity affects the mean duration of active and quiescent periods. Curves show average durations of active and quiescent periods over the simulation of 10 min as a function of synaptic noise intensity. All inhibitory neurons are of LTS type. Synaptic noise intensity varies in the range $0.05 \times 10^{-5} \leq D \leq 5 \times 10^{-5}$ in discrete steps of size $\Delta D = 0.05 \times 10^{-5}$. Error bars: standard error.

The action of synaptic noise upon the average duration of active and quiescent periods can be weaker or stronger depending on the network composition. Although the same common qualitative tendencies persist, many quantitative aspects depend on the types of participating neurons as well as on proportions between them.

An exemplary comparison is shown in Fig 14. Simulations with two types of inhibitory neurons indicate that the LTS neurons, compared to the FS ones, seem to postpone the termination of the active period (top left panel): at low noise the duration of oscillatory activity is higher if LTS neurons are present. This implies that inhibitory neurons influence the transition from active to quiescent period. In contrast, the duration of the quiescent period (bottom right panel) displays no dependence on the type of inhibitory neuron: the corresponding curves in the plot nearly coincide. This indicates that the transition from quiescent to active period is regulated exclusively by excitatory neurons. Indeed, since inhibitory neurons cannot excite a network, every period of stay in the quiescent period should be interrupted by an excitatory neuron, or by a group of excitatory neurons.

Introducing diversity among excitatory neurons, we observe certain quantitative changes as well. By replacing 20% of RS neurons by CH neurons, we obtain a network built of 16%CH, 64%RS and 20%LTS. This composition is much less sensitive to the action of synaptic noise. The tendency of growth of active periods under increase of noise is practically absent (see top left panel in Fig 14), and at all values of D the average active period is shorter than the corresponding silent one. As for the latter, however, there is a systematic shift. Compared to the case when the whole excitatory population is of the RS type, in the mixture with CH neurons the mean duration of quiescent periods decreases to lower values, below 10^2 ms. This decrease is a combination of synaptic noise- and network-related effects. A quiescent period ends whenever synaptic noise or some of the few quiet excitatory neurons which fire during

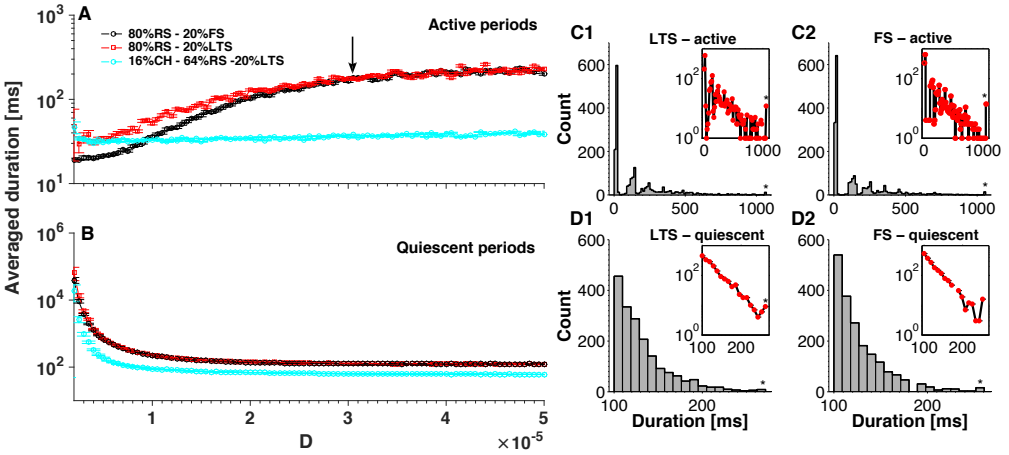

Fig 14. Network composition influences the average duration of stay in active and quiescent periods. A-B: Dependence of duration on noise intensity. Legend in the plot indicates the network composition. Curves: average values over the simulation of 10 min. Error bars: standard error. **A**: active periods. **B**: quiescent periods. The value $D = 3 \times 10^{-5}$, denoted by the arrow, is used for calculation of histograms in panels **C1-2** and **D1-2**, characterizing distributions of stay duration in different periods. Stars at the end of the histograms are outliers. Insets show logarithmic representations of the ordinate.

the quiescent period (or both) drives one of the majority of typical excitatory neurons which are at rest across the firing threshold, provided that this neuron is able to activate its postsynaptic neighbors and initiate thereby a wave of activity. If the neighbors fail to fire, the quiescent period continues. The mean time required for the first neuron to fire is the same for the RS and the CH neuron (see Sect.3.2.1). However, the RS neuron exhibits just one isolated action potential, whereas the CH neuron generates a series of spikes, raising with each of them the conductances of its postsynaptic neighbors and creating thereby conditions for their activation and subsequent collective spiking. In this sense, a burst of a CH neuron has higher chances to initiate common activity than a spike of a RS neuron. Therefore, in a network with CH neurons the quiescent periods end earlier. This confirms our conjecture that excitatory neurons influence the length of quiescent periods.

Histograms of duration of stay in the active period in Figs 14 **C1-2** show exponential distributions but are somehow fractured (cf. the logarithmic representations in the insets). Distributions of this kind have been reported previously [35, 70]. In the former case the authors related cessation of activity to passages through a specific region in the phase space of their deterministic network (the "hole" mentioned above), explaining thereby the quantization of cessation times. In our case, the behavior of the system is similar. Assuming the picture mentioned above of a hole in the network phase space through which the network can escape from active to quiescent state, and a synaptic noise level high enough to allow multiple transitions from quiescent to active state, the quantization of active period durations can be explained keeping in mind that an active period is made of up-down cycles, each one with the same approximate period T. Since the escapes from active to quiescent state always occur at the end of an up-down cycle, the duration of an active state can only increase by integer multiples of T. The distributions of stay duration in the quiescent period, shown in Figs 14 **D1-2**, possess exponential character as well, but without a fractured shape. This can be explained due to the non-oscillatory nature of the quiescent periods.

Let us have a look at shorter timescales: what happens *inside* the active periods? How does noise influence the collective up and down states? In Fig 15 we show average durations of stay in the up and down states as a function of the noise intensity D. The range of noise intensities is the same as the one used in Figs 13 and 14. Whereas the average duration in the down state gets shorter under the growth of noise, the lifetime in the up state almost does not change.

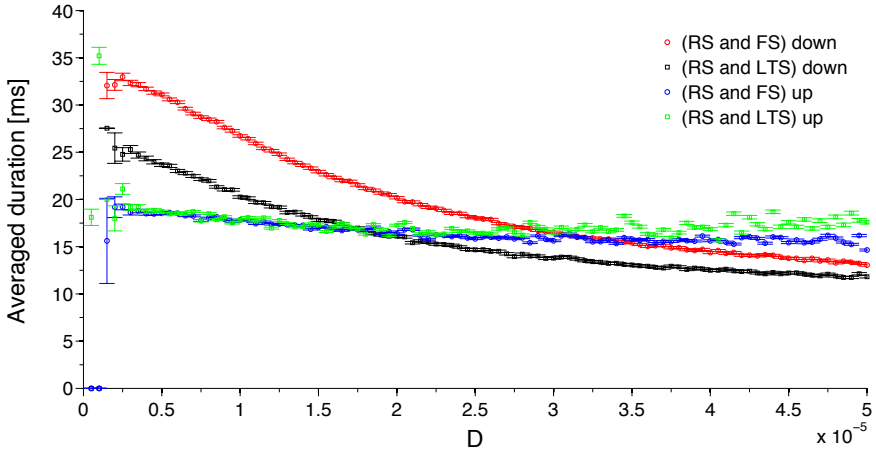

Fig 15. Average duration of stay in the up and down states as a function of noise intensity. The network contains RS excitatory neurons and either FS or LTS inhibitory neurons. Curves: average values over the simulation of 10 min. Error bars: standard error.

The down state is the only state that is sensitive to the type of inhibitory neuron. There is a clear shift upwards (see red and black curves) if the LTS neurons are replaced with FS ones. This means that transitions from the down state happen faster in the presence of LTS neurons. The sensitivity of the down state can be related to the interpretation in [35] where the cessation of self-sustained oscillatory activity was assigned to passages through a small region of instability (the hole), located in the phase space close to the down state. In our current synaptic noise setup, the more noise, the higher the disturbance in the region of instability at the down state and the shorter its lifetime.

4 Discussion

Networks of LIF neurons have been extensively scrutinized in the literature to understand their properties under different conditions [20–22, 24–28, 78–80]. Much fewer works have been devoted to systematic investigations of networks of other spiking neuron models. Here we have studied networks of Izhikevich neurons in the presence of synaptic noise. We have shown that these networks can display a rich variety of activity patterns, consisting of synchronous and asynchronous non-oscillatory states and oscillatory states with variable degrees of synchrony. Moreover, these networks exhibit intermittent noise-induced transitions between oscillatory and quiescent states. These transitions are irregular and affected by the synaptic noise level and the network composition.

A systematic analysis of time series plots of neuron spikes, firing rates, average voltage and membrane recovery variable, and power spectra revealed the characteristics of the oscillatory and quiescent states, similar to observed cortical states [5, 10–13]: in the oscillatory state the membrane voltages of the neurons fluctuate between hyperpolarized (down) and depolarized (up) states as in the so-called "synchronized" states seen in *in vivo* preparations and during slow-wave sleep and anesthesia; in the quiescent state neurons display very low and irregular spiking activity as in the so-called "desynchronized" states seen in quiet rest. As far as we know, phenomena like oscillations between hyperpolarized and depolarized states, and noise-induced intermittent transitions between oscillatory and low activity regimes have not been seen in networks of LIF neurons.

By using the single neuron phase space representation of network dynamics combined with statistical assessments of duration of stay in the oscillatory and quiescent states, we were able to explain the roles played by synaptic noise and network composition in the durations of these states and the transitions between them. Besides, we also were able to explain the origin of the up and down oscillations and the asynchronous non-oscillatory nature of the quiescent states.

Up and down states, which correspond to states where the average voltage of network neurons is respectively depolarized and hyperpolarized, occur during oscillatory (active) periods in our network. They can be understood in terms of the single neuron phase space in the same way we explained in the noiseless case [35]. During an up state, when most of the neurons fire tonically, the voltage nullcline $\bar{u}$ is kept in the upper part of the phase space while the recovery variable u moves steadily upwards due to neuronal firing. Eventually the recovery variable u gets inside the parabolic nullcline $\bar{u}$, which makes the neuron state move to the hyperpolarized region of the phase space and then downwards in a relaxation trajectory towards rest. This corresponds to a down state. In a down state the activity of the network is sustained by quiet neurons, which were inhibited during the up state and became disinhibited during the down state. In the course of time, the firing of quiet neurons is capable of exciting some neurons which are relaxing toward rest and this triggers a new wave of excitation in the network starting another up state. This mechanism strongly depends on the recovery variable u and its instantaneous increment d (cf. Eq.(2)), which causes spike-dependent adaptation [31]. Together, they constitute a sort of intrinsic negative feedback mechanism which decreases network excitability during the up state, as proposed by other authors in different contexts [48, 49, 81–89].

The basic mechanism behind up and down oscillations is present both in the deterministic and the synaptic noise setups. Thus, up-down oscillations are caused not by synaptic noise but by the intrinsic dynamics of the network. Elsewhere, we have shown that networks of AdEx neurons without noise and external inputs also display up-down oscillations [35]. The major difference between the deterministic and the synaptic noise setups is that in the deterministic setup the oscillations are transient,

while in the noisy setup they can be persistent. But the durations of the up and down phases and an up-down cycle are approximately the same, depending only on the intrinsic characteristics of network neurons.

The up-down oscillations can be seen as a sort of default activity mode of the system (at least in the region of the parameter space considered here). In the deterministic, noiseless, setup this activity eventually dies out and we have shown that this is preceded by the passage of the system through a specific region of its phase space we called a "hole" [35]. Through the hole, located close to the domain traversed by the system during a down phase, the system can escape the up-down oscillations and decay to rest. In the noiseless case the system sooner or later gets into the hole and the network activity dies out. In the synaptic noise setup, a hole-like region in the network's high-dimensional stochastic phase space still exists but because of the noise the system does not decay to rest when it passes through it; instead, the system is dragged to the quiescent state.

As in the down state, in the quiescent state the activity of the network is given by the activity internally generated by quiet neurons via their recurrent synaptic connections, which is regulated by the synaptic noise level: for weak synaptic noise the activity is weak, and for strong synaptic noise the activity is strong. Being dictated by noise, activity during a quiescent period is asynchronous and irregular. Because of the passage through the hole the quiescent state has, in general, a longer duration than the down state. Hence, typical neurons which are relaxing in the hyperpolarized region of the single neuron phase space have time to decay to the phase space region around rest. This explains why during quiescent periods the average voltage is close to the resting voltage and is not hyperpolarized as in down states. For weak synaptic noise, activity generated by the quiet neurons is insufficient to take the system out of the quiescent state: the latter and the whole system remains inactive. For moderate to high synaptic noise intensities, the activity of quiet neurons gets stronger and even the neurons that are close to rest can fire, so eventually the global activity is reignited and an up state starts.

The basic effect of the synaptic noise level is to increase/decrease the average duration of the quiescent periods. In other words, synaptic noise can act as a facilitator of transitions between quiescent and active states, and the intermittency between these states results from the stochastic nature of the neuronal firing during quiescent periods as well as of the trajectory of the system in its high-dimensional phase space (which determines whether it will hit a hole or not). Once the system enters the hole, the duration of stay in the quiescent state depends on the noise intensity. For very low noise, the system stays in the quiescent state essentially forever, displaying only residual activity (see Fig 5). For moderate to high noise, the system eventually leaves the quiescent state and the up-down oscillations resume. The residence time in the quiescent state gets smaller as the synaptic noise intensity increases. For very strong noise the system may not even enter the hole because, in such a case, both typical and quiet neurons have high probability of firing at all moments. This explains the disappearance of quiescent periods in the high noise regime. For still higher levels of synaptic noise intensity, even the down periods disappear and the network features having constant activity.

Our study also shows that inhibition affects transitions from active to quiescent periods and the duration of down states. The average duration of down states is shorter when the inhibitory neurons of the network are of the LTS type than when they are of the FS type (cf. Fig 15). This may be related to experimental evidence showing that inhibitory neurons control cortical oscillatory up and down states [61]. The authors of that study progressively blocked inhibitory cells during a spontaneous up state and showed that this blockage shortened the duration of up states and enlarged the duration of down states. Since the LTS neurons respond to noise faster, a replacement of all the

LTS neurons in the network by FS neurons can be viewed as a reduction of inhibition, and therefore the corresponding increase of the average duration of down states relates our observations in the model to the experimental evidence. Similar transitions from the up to the down states have been studied before [48, 74].

For noise, there are many ways to enter a neural network model [37, 38, 42, 90, 91]. In this work we studied the variant in which it is included in the synaptic variables. By doing so, we were able to study the effect of noise at the molecular level on the behavior of the system at the network level. Since noise at the synaptic level is related to fluctuations in the release of neurotransmitters and the amplitude of miniature postsynaptic currents [50, 59, 73], which are phenomena at scales of magnitude much smaller than the scale of voltage changes, the weak noise intensities D we considered here capture very small noisy events. Furthermore, because synaptic noise is filtered by the conductance variables, its effect upon neuronal voltages is akin to colored noise input, which is more biologically realistic than if noise were added, via e.g. Poisson processes, to neuron voltages directly.

Our work captured mechanisms at different levels of neural processing with potential contribution to current endeavors to model multiscale brain mechanisms and their role on normal and pathological function [92–95]. As an example, the synaptic noise-induced switches between periods of oscillatory and irregular activity might give support to fast formation and destruction of cell assemblies, which is a highly influential concept in theoretical neuroscience [96].

5 Supporting information

S1 Fig. Transient up-down oscillations in the weak synaptic noise setup. Network composition: 16%CH, 64%RS and 20%LTS neurons. Synaptic increments: $(g_{\text{ex}}, g_{\text{in}}) = (0.15, 1)$. Intensity of synaptic noise: $D = 2.5 \times 10^{-6}$. The network received a brief external stimulus from the beginning of simulation until $t = 80$ ms. After this the network was left to evolve freely until the end of the simulation. Upper panel: raster plot showing the firing activity in the network for $t \geq 100$ ms, so after the end of external input. The raster plot is divided into 6 time intervals Δt_i with duration 100 ms each. The network displays oscillatory behavior for a transient period followed by a quiescent state that lasts until the end of simulation. Lower panels: voltage series and dynamics on the phase plane of an arbitrary selected neuron in subsequent intervals Δt_i. Blue dashed line: the first 50 ms of evolution. Blue solid line: the last 50 ms of evolution. Red circle: location of the neuron at the end of the time interval. Black square: location of the state of rest with $v = v_{\text{rest}}$ and $u = u_{\text{rest}}$. Dotted red lines: reset value of voltage and spike cutoff. Green lines: Nullclines $\bar{u}$ and u^*, according to Eq (11). The location of the parabolic nullcline $\bar{u}$ is time-dependent; its position at the beginning (respectively, end) of Δt_i is shown with dashed (respectively, solid) green line.

6 Acknowledgments

We are thankful to P. Tomov for stimulating discussions. Our research is supported by FAPESP 2015/50122-0 and DFG-IRTG 1740. RP and ACR are also part of the Research, Innovation and Dissemination Center for Neuromathematics (FAPESP grant 2013/07699-0). RP is supported by a FAPESP scholarship (2013/25667-8). ACR is partially supported by a CNPq fellowship (grant 306251/2014-0).

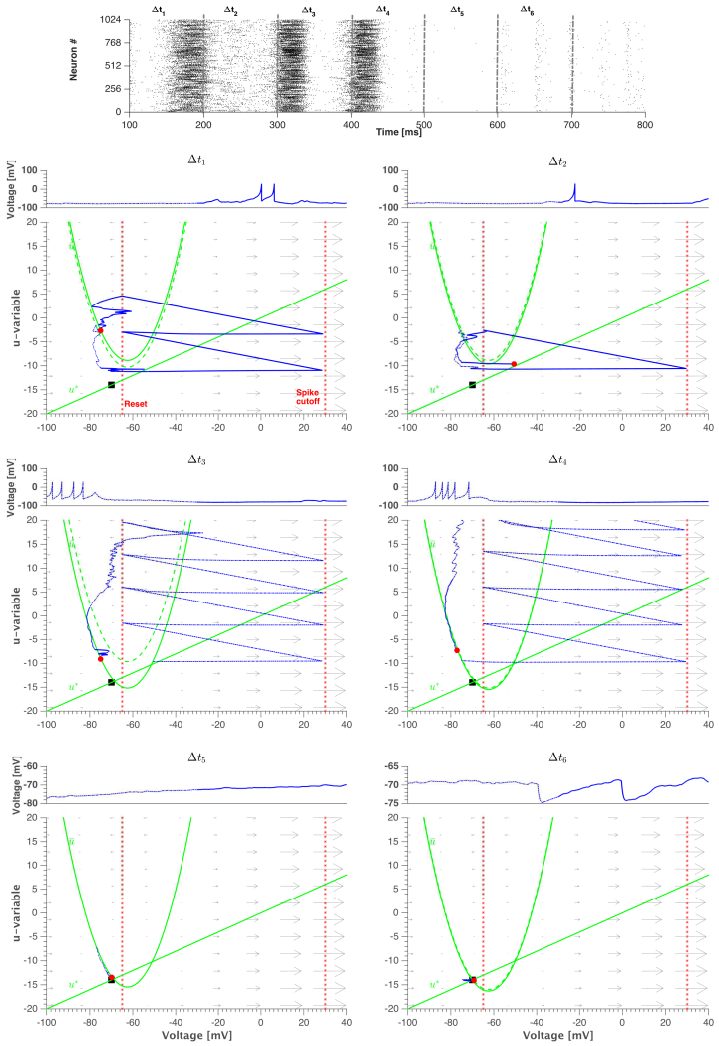

References

1. Buzsaki G, Draguhn A. Neuronal oscillations in cortical networks. Science. 2004;304:1926-1929.

2. Bonifazi P, Goldin M, Picardo MA, Jorquera I, Cattani A, Bianconi G, Represa A, Ben-Ari Y, Cossart R. GABAergic hub neurons orchestrate synchrony in developing hippocampal networks. Science. 2009;326:1419-1424.

3. Uhlhaas PJ, Pipa G, Lima B, Melloni L, Neuenschwander S, Nikolić D, Singer W. Neural synchrony in cortical networks: history, concept and current status. Frontiers in Integrative Neuroscience. 2009;3:17.

4. Colgin LL. Oscillations and hippocampal-prefrontal synchrony. Current Opinion in Neurobiology. 2011;21:467–474.

5. Harris KD, Thiele A. Cortical state and attention. Nature Reviews Neuroscience. 2011;12:509–523.

6. Vyazovskiy VV, Olcese U, Hanlon EC, Nir Y, Cirelli C, Tononi G. Local sleep in awake rats. Nature. 2011;472:443–447.

7. Sachidhanandam S, Sreenivasan V, Kyriakatos A, Kremer Y, Petersen CCH Membrane potential correlates of sensory perception in mouse barrel cortex. Nature Neuroscience. 2013;16:1671–1677.

8. Miller JK, Ayzenshtat I, Carrillo-Reid L, Yuste R. Visual stimuli recruit intrinsically generated cortical ensembles. Proceedings of the National Academy of Sciences (USA). 2014;111:E4053–E4061.

9. Okun M, Steinmetz NA, Cossell L, Florencia Iacaruso M, Ko H, Barthó P, Moore T, Hofer SB, Mrsic-Flogel TD, Carandini M, Harris KD. Diverse coupling of neurons to populations in sensory cortex. Nature. 2015;521:511–515.

10. Steriade M, Timofeev I, Grenier F. Natural waking and sleep states: a view from inside neocortical neurons. Journal of Neurophysiology. 2001;85:1969–1985.

11. El Boustani S, Popischil M, Rudolph-Lilith M, Destexhe A. Activated cortical states: Experiments, analyses and models. Journal of Physiology (Paris). 2007;101:99–109.

12. Greenberg DS, Houweling AR, Kerr JN. Population imaging of ongoing neuronal activity in the visual cortex of awake rats. Nature Neuroscience. 2008;11:749–751.

13. Sanchez-Vives MV, Massimini M, Mattia M. Shaping the default activity patterns of the cortical network. Neuron. 2017;94:993–1001.

14. Ahn S, Rubchinsky LL. Short desynchronization episodes prevail in synchronous dynamics of human brain rhythms. Chaos: An Interdisciplinary Journal of Nonlinear Science. 2013;23:013138.

15. Ahn S, Rubchinsky LL. Potential mechanisms and functions of intermittent neural synchronization. Frontiers in Computational Neuroscience. 2017;11:44.

16. Hahn G, Ponce-Alvarez A, Monier C, Benvenuti G, Kumar A, Chavane F, Deco G, Frégnac Y. Spontaneous cortical activity is transiently poised close to criticality. PLoS Computational Biology. 2017;13:e1005543.

17. van Vreeswijk C, Sompolinsky H. Chaos in neuronal networks with balanced excitatory and inhibitory activity. Science. 1996;274:1724–1726.

18. Amit DJ, Brunel N. Model of global spontaneous activity and local structured activity during delay periods in the cerebral cortex. Cerebral Cortex. 1997;7:237–252.

19. Renart A, de la Rocha J, Bartho P, Hollender L, Parga N, Reyes A, Harris KD. The asynchronous state in cortical circuits. Science. 2010;327:587–590.

20. Landau ID, Egger R, Dercksen VJ, Oberlaender M, Sompolinsky H. The impact of structural heterogeneity on excitation-inhibition balance in cortical networks. Neuron. 2016;92:1106–1121.

21. Brunel N. Dynamics of sparsely connected networks of excitatory and inhibitory spiking neurons. Journal of Computational Neuroscience. 2000;8:183–208.

22. Vogels TP, Abbott LF. Signal propagation and logic gating in networks of integrate-and-fire neurons. Journal of Neuroscience. 2005;25:10786–10795.

23. Kumar A, Schrader S, Aertsen A, Rotter S. The high-conductance state of cortical networks. Neural Computation. 2008;20:1–43.

24. Wang SJ, Hilgetag CC, Zhou C. Sustained activity in hierarchical modular neural networks: self-organized criticality and oscillations. Frontiers in Computational Neuroscience. 2011;5:30.

25. Litwin-Kumar A, Doiron B. Slow dynamics and high variability in balanced cortical networks with clustered connections. Nature Neuroscience. 2012;15:1498–1505.

26. Kriener B, Enger H, Tetzlaff T, Plesser HE, Gewaltig MO, Einevoll GT Dynamics of self-sustained asynchronous-irregular activity in random networks of spiking neurons with strong synapses. Frontiers in Computational Neuroscience. 2014;8:136.

27. Ostojic S. Two types of asynchronous activity in networks of excitatory and inhibitory spiking neurons. Nature Neuroscience. 2014;17:594–600.

28. Potjans TC, Diesmann M. The cell-type specific cortical microcircuit: relating structure and activity in a full-scale spiking network model. Cerebral Cortex. 2014;24:785–806.

29. Vogels TP, Rajan K, Abbott LF. Neural network dynamics. Annual Review of Neuroscience. 2005;28:357–376.

30. Izhikevich EM. Simple model of spiking neurons. IEEE Transactions on Neural Networks. 2003;14:1569–1572.

31. Izhikevich EM. Dynamical Systems in Neuroscience: The Geometry of excitability and Bursting. Cambridge, MA: MIT Press; 2007.

32. Brette R, Gerstner W. Adaptive exponential integrate-and-fire model as an effective description of neuronal activity. Journal of Neurophysiology. 2005;94:3637–3642.

33. Gerstner W, Kistler WM, Naud R, Paninski L. Neuronal Dynamics: from Single Neurons to Networks and Models of Cognition. Cambridge, UK: Cambridge University Press; 2014.

34. Tomov P, Pena RFO Zaks MA Roque AC. Sustained oscillations, irregular firing, and chaotic dynamics in hierarchical modular networks with mixtures of electrophysiological cell types. Frontiers in Computational Neuroscience. 2014;8:103.

35. Tomov P, Pena RFO, Roque AC, Zaks MA. Mechanisms of self-sustained oscillatory states in hierarchical modular networks with mixtures of electrophysiological cell types. Frontiers in Computational Neuroscience. 2016;10:23.

36. Shadlen MN, Newsome WT. Noise, neural codes and cortical organization. Current Opinion in Neurobiology. 1994;4:569–579.

37. Faisal AA, Selen LP, Wolpert DM. Noise in the nervous system. Nature Reviews Neuroscience. 2008;9:292–303.

38. Longtin A. Neuronal noise. Scholarpedia. 2013;8(9):1618.

39. Stiefel KM, Englitz B, Sejnowski TJ Origin of intrinsic irregular firing in cortical interneurons. Proceedings of the National Academy of Sciences (USA). 2013;110:7886–7891.

40. Hartmann C, Lazar A, Nessler B, Triesch J. Where's the noise? Key features of spontaneous activity and neural variability arise through learning in a deterministic network. PLoS Computational Biology. 2015;11:e1004640.

41. Maass W. Searching for principles of brain computation. Current Opinion in Behavioral Sciences. 2016;11:81–92.

42. Destexhe A, Rudolph-Lilith M. Neuronal Noise. New York, NY: Springer; 2012.

43. Petersen CCH, Hahn TTG, Mehta M, Grinvald A, Sakmann B. Interaction of sensory responses with spontaneous depolarization in layer 2/3 barrel cortex. Proceedings of the National Academy of Sciences (USA). 2003;100:13638–13643.

44. Haider B, Duque A, Hasenstaub AR, Yu Y, McCormick DA. Enhancement of visual responsiveness by spontaneous local network activity in vivo. Journal of Neurophysiology. 2007;97:4186–4202.

45. Cossart R, Aronov D, Yuste R. Attractor dynamics of network UP states in the neocortex. Nature. 2003;423:283–288.

46. Seamans JK, Nogueira L, Lavin A. Synaptic basis of persistent activity in prefrontal cortex *in vivo* and in organotypic cultures. Cerebral Cortex. 2003;13:1242–1250.

47. Shu Y, Hasenstaub A, Badoual M, Bal T, McCormick DA. Barrages of synaptic activity control the gain and sensitivity of cortical neurons. Journal of Neuroscience. 2003;23:10388–10401.

48. Holcman D, Tsodyks M. The emergence of Up and Down states in cortical networks. PLoS Computational Biology. 2006;2:e23.

49. Parga N, Abbott LF. Network model of spontaneous activity exhibiting synchronous transitions between up and down states. Frontiers in Neuroscience. 2007;1:57–66.

50. Liu ZW, Faraguna U, Cirelli C, Tononi G, Gao XB. Direct evidence for wake-related increases and sleep-related decreases in synaptic strength in rodent cortex. Journal of Neuroscience. 2010;30:8671–8675.

51. Montoro AMG, Cao R, Espinosa N, Cudeiro J, Mariño J. Functional two-way analysis of variance and bootstrap methods for neural synchrony analysis. BMC Neuroscience. 2014;15:96.

52. Ginzburg I, Sompolinsky H. Theory of correlations in stochastic neural networks. Physical review E. 1994;50:3171–3191.

53. Lo CC, Amaral LN, Havlin S, Ivanov PC, Penzel T, Peter JH, Stanley HE. Dynamics of sleep-wake transitions during sleep. Europhysics Letters. 2002;57:625.

54. Behn CGD, Brown EN, Scammell TE, Kopell NJ. Mathematical model of network dynamics governing mouse sleep–wake behavior. Journal of Neurophysiology. 2007;97:3828–3840.

55. Liu X, Yanagawa T, Leopold DA, Chang C, Ishida H, Fujii N, Duyn JH. Arousal transitions in sleep, wakefulness, and anesthesia are characterized by an orderly sequence of cortical events. Neuroimage. 2015;116:222–231.

56. Abbott L, van Vreeswijk C. Asynchronous states in networks of pulse-coupled oscillators. Physical Review E. 1993;48:1483–1490.

57. Girones Z, Destexhe, A. Enhanced responsiveness in asynchronous irregular neuronal networks. arXiv preprint. 2016;1611.09089.

58. de Kock CP, Sakmann B. Spiking in primary somatosensory cortex during natural whisking in awake head-restrained rats is cell-type specific. Proceedings of the National Academy of Sciences (USA). 2009;106:16446–16450.

59. Tononi G, Cirelli C. Sleep and the price of plasticity: from synaptic and cellular homeostasis to memory consolidation and integration. Neuron. 2014;81:12–34.

60. Haider B, Häusser M, Carandini M. Inhibition dominates sensory responses in the awake cortex. Nature. 2013;493:97–100.

61. Sanchez-Vives MV, Mattia M, Compte A, Perez-Zabalza M, Winograd M, Descalzo VF, Reig R. Inhibitory modulation of cortical up states. Journal of Neurophysiology. 2010;104:1314–1324.

62. Benzi R, Sutera A, Vulpiani A. The mechanism of stochastic resonance. Journal of Physics A. 1981;14:L453–L457.

63. Destexhe A, Rudolph M, Fellous JM, Sejnowski TJ. Fluctuating synaptic conductances recreate in vivo-like activity in neocortical neurons. Neuroscience. 2001;107:13–24.

64. Gillespie DT. The mathematics of Brownian motion and Johnson noise. American Journal of Physics. 1996;64:225–239.

65. Uhlenbeck GE, Ornstein LS. On the theory of the Brownian motion. Physical Review. 1930;36:823–841.

66. Mannella R. Integration of stochastic differential equations on a computer. International Journal of Modern Physics C. 2002;13:1177–1194.

67. Sahasranamam A, Vlachos I, Aertsen A, Kumar A. Dynamical state of the network determines the efficacy of single neuron properties in shaping the network activity. Scientific Reports. 2016;6.

68. Blanco S, Garay A, Coulombie D. Comparison of frequency bands using spectral entropy for epileptic seizure prediction. ISRN Neurology. 2013;287327.

69. Young GA, Steinfels GF, Khazan N, Glaser EM. Cortical EEG power spectra associated with sleep-awake behavior in the rat. Pharmacology Biochemistry and Behavior. 1978;8:89–91.

70. Duc KD, Parutto P, Chen X, Epsztein J, Konnerth A, Holcman D. Synaptic dynamics and neuronal network connectivity are reflected in the distribution of times in Up states. Frontiers in Computational Neuroscience. 2015;9:96.

71. Wilson C. Up and down states. Scholarpedia. 2008;3(6):1410.

72. Siegert AJ. On the first passage time probability problem. Physical Review. 1951;81:617–623.

73. Rao Y, Liu ZW, Borok E, Rabenstein RL, Shanabrough M, Lu M, Picciotto MR, Horvath TL, Gao XB. Prolonged wakefulness induces experience-dependent synaptic plasticity in mouse hypocretin/orexin neurons. Journal of Clinical Investigation. 2007;117:4022–4033.

74. Xu X, Ni L, Wang R. A neural network model of spontaneous up and down transitions. Nonlinear Dynamics. 2016;84:1541–1551.

75. Nowak LG, Azouz R, Sanchez-Vives MV, Gray CM, McCormick DA. Electrophysiological classes of cat primary visual cortical neurons in vivo as revealed by quantitative analyses. Journal of Neurophysiology. 2003;89:1541–1566.

76. Contreras, D. Electrophysiological classes of neocortical neurons. Neural Networks. 2004;17:633–646.

77. Maimon G, Assad JA. Beyond Poisson: increased spike-time regularity across primate parietal cortex. Neuron. 2009;62:426–440.

78. Cessac B, Viéville T. On dynamics of integrate-and-fire neural networks with conductance based synapses. Frontiers in Computational Neuroscience. 2008;2:2.

79. Mattia M, Del Giudice P. Population dynamics of interacting spiking neurons. Physical review E. 2002;66:051917.

80. Yim MY, Kumar A, Aertsen A, Rotter S. Impact of correlated inputs to neurons: modeling observations from *in vivo* intracellular recordings. Journal of Computational Neuroscience. 2014;37:293–304.

81. Jercog D, Roxin A, Barthó P, Luczak A, Compte A, de la Rocha J. UP-DOWN cortical dynamics reflect state transitions in a bistable network. eLIFE. 2017;6:e22425.

82. Contreras D, Timofeev I, Steriade M. Mechanisms of long-lasting hyperpolarizations underlying slow sleep oscillations in cat corticothalamic networks. Journal of Physiology (London). 1996;494:251-264.

83. Sanchez-Vives MV, McCormick DA. Cellular and network mechanisms of rhythmic recurrent activity in neocortex. Nature Neuroscience. 2000;3:1027–1034.

84. Bazhenov M, Timofeev I, Steriade M, Sejnowski TJ. Model of thalamocortical slow-wave sleep oscillations and transitions to activated states. Journal of Neuroscience. 2002;22:8691–8704.

85. Benita JM, Guillamon A, Deco G, Sanchez-Vives MV. Synaptic depression and slow oscillatory activity in a biophysical network model of the cerebral cortex. Frontiers in Computational Neuroscience 2012;6:64.

86. Chen JY, Chauvette S, Skorheim S, Timofeev I, Bazhenov M. Interneuron-mediated inhibition synchronizes neuronal activity during slow oscillation. Journal of Physiology (London). 2012;590:3987—4010.

87. Compte A, Sanchez-Vives MV, McCormick DA, Wang XJ. Cellular and network mechanisms of slow oscillatory activity (¡1 Hz) and wave propagations in a cortical network model. Journal of Neurophysiology 2003;89:2707—2725.

88. Ghorbani M, Mehta M, Bruinsma R, Levine AJ. Nonlinear-dynamics theory of up-down transitions in neocortical neural networks. Physical Review E 2012;85:021908.

89. Hill S, Tononi G. Modeling sleep and wakefulness in the thalamocortical system. Journal of Neurophysiology 2005;93:1671—1698.

90. Brochini L, de Andrade Costa A, Abadi M, Roque AC, Stolfi J, Kinouchi O. Phase transitions and self-organized criticality in networks of stochastic spiking neurons. Scientific Reports 2016;6:35831.

91. McDonnell MD, Goldwyn JH, Lindner B. Editorial: Neuronal stochastic variability: Influences on spiking dynamics and network activity. Frontiers in Computational Neuroscience 2016;10:38.

92. Lytton WW, Arle J, Bobashev G, Ji S, Klassen TL, Marmarelis VZ, Schwaber J, Sherif MA, Sanger TD. Multiscale modeling in the clinic: diseases of the brain and nervous system Brain Informatics 2017;https://doi.org/10.1007/s40708-017-0067-5.

93. Neymotin SA, McDougal RA, Bulanova AS, Zeki M, Lakatos P, Terman D, Hines ML, Lytton WW. Calcium regulation of HCN channels supports persistent activity in a multiscale model of neocortex Neuroscience 2016;316:344–366.

94. Mejias JF, Murray JD, Kennedy H, Wang XJ. Feedforward and feedback frequency-dependent interactions in a large-scale laminar network of the primate cortex Science Advances 2016;2:e1601335.

95. Schwalger T, Deger M, Gerstner W. Towards a theory of cortical columns: from spiking neurons to interacting neural populations of finite size PLoS Computational Biology 2017;13:e1005507.

96. Abeles M. Cell assemblies. Scholarpedia 2011;6(7):1505.